Inheritance of cortical ER in yeast is required for normal septin organization

Christopher J.R. Loewen,[1,2,3] Barry P. Young,[2,3] Shabnam Tavassoli,[2,3] and Timothy P. Levine[1]

[1]Division of Cell Biology, University College London Institute of Ophthalmology, London EC1V 9EL, England, UK
[2]Department of Cellular and Physiological Sciences and [3]Brain Research Centre, Life Sciences Institute, University of British Columbia, Vancouver, British Columbia V6T 1Z3, Canada

How cells monitor the distribution of organelles is largely unknown. In budding yeast, the largest subdomain of the endoplasmic reticulum (ER) is a network of cortical ER (cER) that adheres to the plasma membrane. Delivery of cER from mother cells to buds, which is termed cER inheritance, occurs as an orderly process early in budding. We find that cER inheritance is defective in cells lacking Scs2, a yeast homologue of the integral ER membrane protein VAP (vesicle-associated membrane protein–associated protein) conserved in all eukaryotes. Scs2 and human VAP both target yeast bud tips, suggesting a conserved action of VAP in attaching ER to sites of polarized growth. In addition, the loss of either Scs2 or Ice2 (another protein involved in cER inheritance) perturbs septin assembly at the bud neck. This perturbation leads to a delay in the transition through G2, activating the *Saccharomyces* wee1 kinase (Swe1) and the morphogenesis checkpoint. Thus, we identify a mechanism involved in sensing the distribution of ER.

Introduction

Although the distributions of intracellular organelles in each cell type are highly complex, very few mechanisms have been discovered by which a cell might sense and respond to the incorrect or correct position of an organelle (Sutterlin et al., 2002). The budding yeast *Saccharomyces cerevisiae* is an excellent model to study the distribution of organelles because they move into the bud and duplicate in a predictable manner coordinated with the cell cycle. In G1, polarized growth commences after bud site selection; in S phase, small buds grow by the accumulation of organelles and other components made in the mother cell. In G2, the actin cytoskeleton depolarizes, leading to a switch from apical to isotropic (equal in all directions) growth with autonomous production of organelles in the bud. Finally, in M phase, buds acquire a copy of the genome and participate in cytokinesis. Progress through budding is monitored by checkpoints analogous to nuclear checkpoints that relay information to the nucleus, delaying cell cycle progression if bud formation is defective. To date, aspects known to be monitored include cell wall deposition (Suzuki et al., 2004), the actin cytoskeleton (McMillan et al., 1998), and the septin collar at the bud neck (Barral et al., 1999; Longtine et al., 2000). The latter two pathways both activate Swe1 (the *Saccharomyces* wee1 homologue), which inhibits Cdc28 (the *Saccharomyces* cdk1 homologue) to delay the G2→M transition, a mechanism that has been called the morphogenesis checkpoint (Lew, 2003).

The ER in yeast consists of the nuclear envelope and a network lying just beneath the plasma membrane called the cortical ER (cER), with a few cytoplasmic ER tubules linking these two domains (Voeltz et al., 2002). Similar cER exists in all higher eukaryotic cells, with specific functions in calcium signaling and lipid traffic (Berridge, 2002). In yeast, the plasma membrane has multiple focal attachments to a portion of the cER that is biochemically specialized for synthesizing plasma membrane lipids (Pichler et al., 2001). ER inheritance can be divided into three distinct phases: first, cytoplasmic ER tubules move into small buds along actin cables over the relatively long distance of the mother-bud axis; second, the first domain of cER forms by attachment to plasma membrane at the bud tip; and third, cER spreads around the entire bud to form a polygonal tubular network (Fehrenbacher et al., 2002; Du et al., 2006). The attachment step is potentially facilitated by the interaction of translocon components (Sbh1 and Sbh2) and reticulons (Rtn1, Rtn2, and Yop1) on the ER with exocyst components (Sec3, Sec6, and Sec8) on the plasma membrane, without which cER inheritance is delayed (Wiederkehr et al., 2003; Reinke et al., 2004; De Craene et al., 2006). Other proteins implicated in ER

Correspondence to Timothy P. Levine: tim.levine@ucl.ac.uk

Abbreviations used in this paper: cER, cortical ER; HU, hydroxyurea; SGA, synthetic genetic array; TMD, transmembrane domain; VAP, vesicle-associated membrane protein–associated protein.

The online version of this article contains supplemental material.

The Journal of Cell Biology, Vol. 179, No. 3, November 5, 2007 467–483
http://www.jcb.org/cgi/doi/10.1083/jcb.200708205

inheritance include Swa2 (also called Aux1), which unfolds clathrin (Du et al., 2001); Ypt11, a Rab protein on the ER (Buvelot Frei et al., 2006); Ptc1 and Nbp2, which are regulators of MAPK signaling (Du et al., 2006); Ice2, an integral ER membrane protein of unknown function (Estrada de Martin et al., 2005); and the motor Myo4 and its adaptor She3, which are thought to carry ER tubules into the bud (Estrada et al., 2003).

VAP (vesicle-associated membrane protein–associated protein) is a small, highly conserved integral ER protein (Skehel et al., 1995). The major VAP homologue in yeast, Scs2 (Loewen and Levine, 2005), interacts with a large number of other proteins (Gavin et al., 2002; Loewen et al., 2003). Some of these, including the sterol transfer proteins Osh2 and Osh3, are on the plasma membrane (Levine and Munro, 2001), where they are restricted by Scs2 to those parts of the plasma membrane with subjacent cER (Loewen et al., 2003). This suggests that Scs2 complexes bridge from cER to the plasma membrane and led us to ask whether Scs2 has a role in forming cER. We report now that the amount of cER is reduced ∼50% in cells lacking Scs2, with buds more affected than mother cells. Scs2 interacts with an unidentified receptor localized to sites of polarized growth, indicating a role for Scs2 in attaching cER to bud tips. In addition, we found that *SCS2* interacts genetically with *ICE2* and that defects in either gene, and especially both in combination, disrupt septins at the bud neck, which triggers the morphogenesis checkpoint.

Results

cER is disrupted by the loss of Scs2

To examine the role of VAP on ER structure, we examined the effect of Δscs2 deletion on a fluorescent ER marker in live cells. Confocal sections of wild-type cells expressing the reporter showed the typical pattern of nuclear envelope, occasional cytoplasmic strands, and an extensive network of cER (Fig. 1 A and Fig. S1, available at http://www.jcb.org/cgi/content/full/jcb.200708205/DC1). Qualitatively cER formed an incomplete circle, and quantitatively cER was subjacent to 72% of plasma membrane (Fig. S1). In *Δscs2* cells, qualitatively cER rarely formed circles, and quantitatively cER was present in 37% of the periphery (Figs. 1 B and S1). The reporter used, RFP-ER, contains the transmembrane domain (TMD) of Scs2. In case this had unforeseen interactions, we performed similar studies with two other ER reporters tagged with GFP. Are2, an ER resident enzyme with multiple TMDs (Zweytick et al., 2000), was present at 39% of the periphery in *Δscs2* cells compared with 77% in wild type, and the C-terminal domain of Sec12, which includes a single TMD specifying ER localization (Sato et al., 1996), was at 33% of the periphery in *Δscs2* cells compared with 57% in wild type (Fig. S1). In addition, we used an automated method to process images of cells coexpressing RFP-ER with plasma membrane–targeted GFP. The proportion of total ER colocalized with the plasma membrane fell from 50.3% in wild-type cells to 25.6% in *Δscs2* cells, which is a relative decrease of 49% (Fig. S2, A and B). Thus, three different ER-targeted reporters showed reductions of ∼50% in the amount of cER upon the loss of Scs2.

We next assessed whether *Δscs2* affects cER inheritance, which is indicated by a stronger phenotype in buds than mothers (Du et al., 2004). In mother cells with identifiable buds, the deletion of *SCS2* disproportionately affected the levels of cER in buds compared with mother cells (Fig. 1, C–E). This effect of *Δscs2* was found in different yeast strains (unpublished data) and was not enhanced by further deletion of the homologue *SCS22* (unpublished data).

To validate these results, we performed thin section EM on a strain in which Scs2 levels are regulated by carbon source (Loewen et al., 2003). Repression of *SCS2* (here referred to as *scs2^r*) reduced cER in unbudded profiles by 53% (Fig. 2, A, B, and E), verifying the findings with fluorescent markers. This excludes an alternate possibility that in *Δscs2*, cER is present in normal quantity but with reduced access. Looking next at budded profiles, we found that *scs2^r* had a far stronger effect in buds (31% of the amount of cER compared with wild type) than in mothers (55%; Fig. 2, C, D, and F), confirming that Scs2 has a role in cER inheritance. We also examined two other aspects of ER morphology in *Δscs2* cells. First, where cER formed, its morphology as a tubular network was essentially preserved (Fig. S2 C), ruling out an effect similar to the overexpression of reticulons (De Craene et al., 2006; Voeltz et al., 2006). Second, the overall amount of ER in buds (i.e., including cytoplasmic tubules) was not affected by *Δscs2* (Fig. S2 D). Thus, Scs2 is required for formation of the correct attachment of cytoplasmic ER to the periphery to make cER but not for transport of cytoplasmic ER into buds or for microanatomy of the cER network.

SCS2 interacts with *ICE2* in cER inheritance

We next compared *Δscs2* cells with strains carrying one of four other mutations that affect cER inheritance: *Δshe3*, *Δmyo4*, *Δswa2*, and *Δice2* (Du et al., 2001; Estrada et al., 2003; Estrada de Martin et al., 2005). cER in our *Δshe3*, *Δmyo4*, *Δswa2*, and *Δice2* strains appeared normal (Fig. S3 A, available at http://www.jcb.org/cgi/content/full/jcb.200708205/DC1). This lack of effect is compatible with the original studies implicating these genes in cER inheritance because there the gene deletions caused only minor delays in cER inheritance, which are strain dependent (Estrada et al., 2003; Reinke et al., 2004). We also combined *Δscs2* with the other deletions to indicate genes acting in common pathways. cER in *Δmyo4Δscs2*, *Δshe3Δscs2*, and *Δswa2Δscs2* cells was not distinguishable from *Δscs2* cells (Fig. S3 B and not depicted). In comparison, we failed to introduce *Δscs2* directly into a *Δice2* strain by PCR, which is consistent with the aggravating genetic interaction noted previously in a large-scale genetic study (Schuldiner et al., 2005). To examine this interaction, we introduced repressible *SCS2* (*scs2^r*; Loewen et al., 2003) into a *Δice2* strain. *Δice2scs2^r* cells, which grew slowly (not depicted), contained less cER than either *scs2^r* or *Δscs2*, particularly in buds (Fig. 3 A), where cytoplasmic ER often accumulated in a punctum at some distance from the bud tip (Fig. 3 B). A similar pattern was seen rarely in *Δscs2* cells but not in *Δice2* (unpublished data).

Synthetic genetic array (SGA) analysis for both *SCS2* and *ICE2* with known nonessential genes implicated in cER inheritance identified a genetic interaction between *SCS2* and

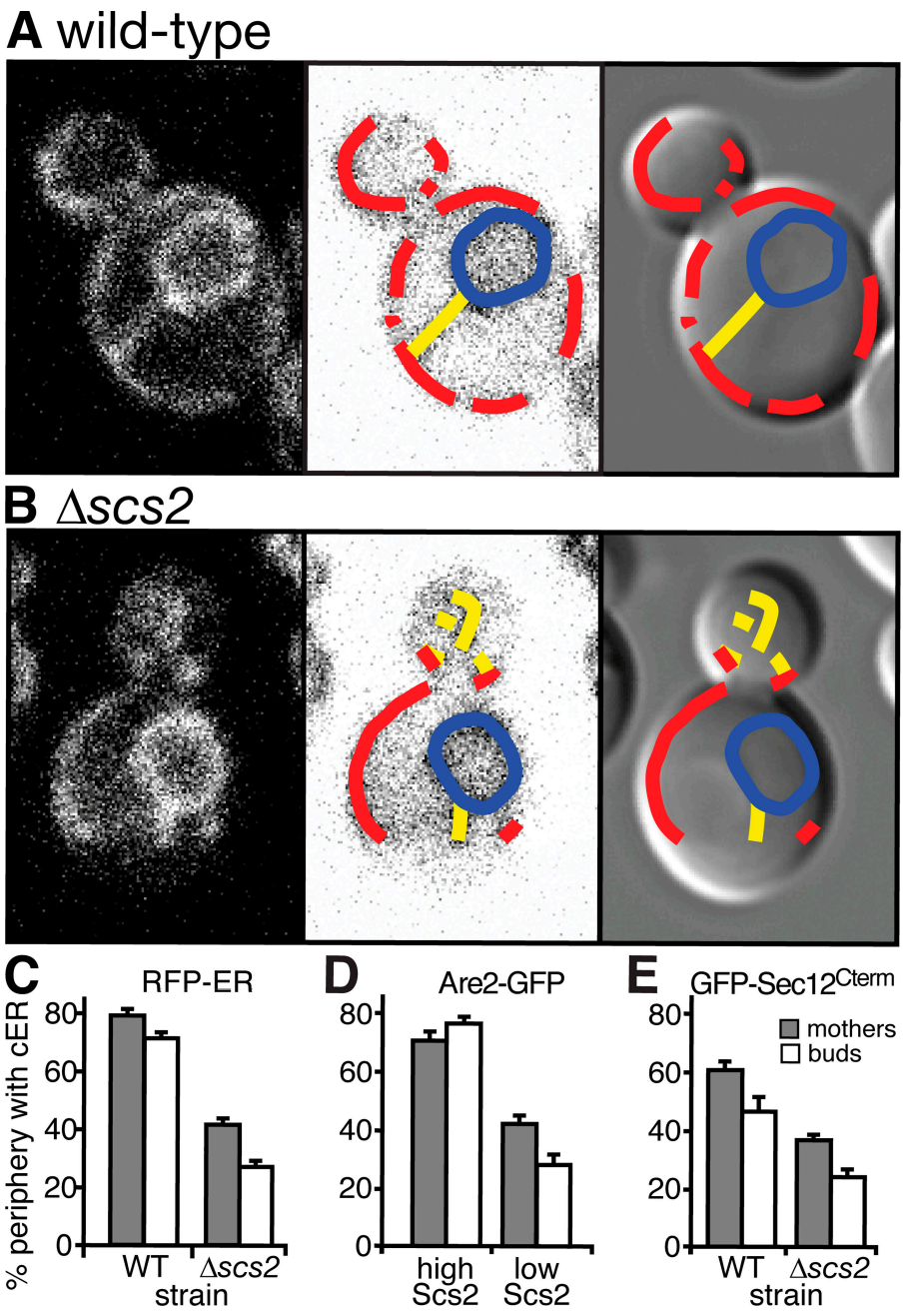

Figure 1. **Role of Scs2 in the formation of cER.** (A and B) cER is reduced by *Δscs2*. Single typical wild-type (A) and *Δscs2* (B) cells expressing RFP-ER, a fluorescent reporter for ER membranes, with a cER amount close to the population means. Fluorescence images (left) and transmission images (right) are accompanied by inverted fluorescence images (middle) on which the three subdomains of ER are drawn: nuclear envelope (blue), cytoplasmic (yellow), and cER (red). The proportion of cell periphery with cER in the mother and bud is 63% and 66% (A) and 40% and 16% (B), respectively. (C–E) Quantitative effect of altered levels of Scs2 on cER assessed by fluorescence microscopy. The proportion of cell perimeter with associated cER was assessed for populations of mothers and buds separately using three different markers of the ER: RFP-ER (C), Are2-GFP (D), and GFP-Sec12 C-terminal domain (Sec12^{Cterm}; E). In C and E, wild-type cells were compared with *Δscs2* cells. In D, TLY251 cells were grown to induce or repress *SCS2*. Error bars indicate SEM.

ICE2 (Fig. 3 C). Aggravating genetic interactions were also found between these genes and *PTC1* and *NBP2*, regulators of MAPK pathways that are important for moving ER tubules into the bud (Du et al., 2006). This provides additional evidence that Scs2 and Ice2 function in attachment of the ER to the cortex. Conversely, the growth defect of *Δice2* was alleviated by the deletion of reticulons, chiefly Rtn1; an alleviating interaction between *Δscs2* and *Δrtn1* could not have been reported in our experiment because neither single deletion reduced the growth rate. The interaction between *SCS2* and *ICE2* was confirmed by tetrad analysis and growth assay of the double mutant on synthetic defined medium (Fig. 3 D). Interestingly, this phenotype was less severe on rich medium, an effect we have yet to understand. On both media, these cells had reduced cER similar to *Δice2scs2^{r}* cells (unpublished data). Overall, these results indicate that Ice2 and Scs2 act in parallel pathways, without which cytoplasmic ER enters buds but fails to attach to the bud tip.

Scs2 and human VAP-A/B target sites of polarized growth

If Scs2, an integral ER protein, mediates the attachment of ER to the bud tip, is it possible that Scs2 interacts with a component at the bud tip? To examine this possibility, we expressed Scs2 lacking its C-terminal TMD and tagged with GFP (Scs2ΔTMD-GFP), which might be expected to be uniformly cytosolic, as is GFP. Instead, Scs2ΔTMD-GFP targeted specific extranuclear sites, including tips of small buds and sites of recent cell division (the incipient bud site), which are both sites of polarized growth, in

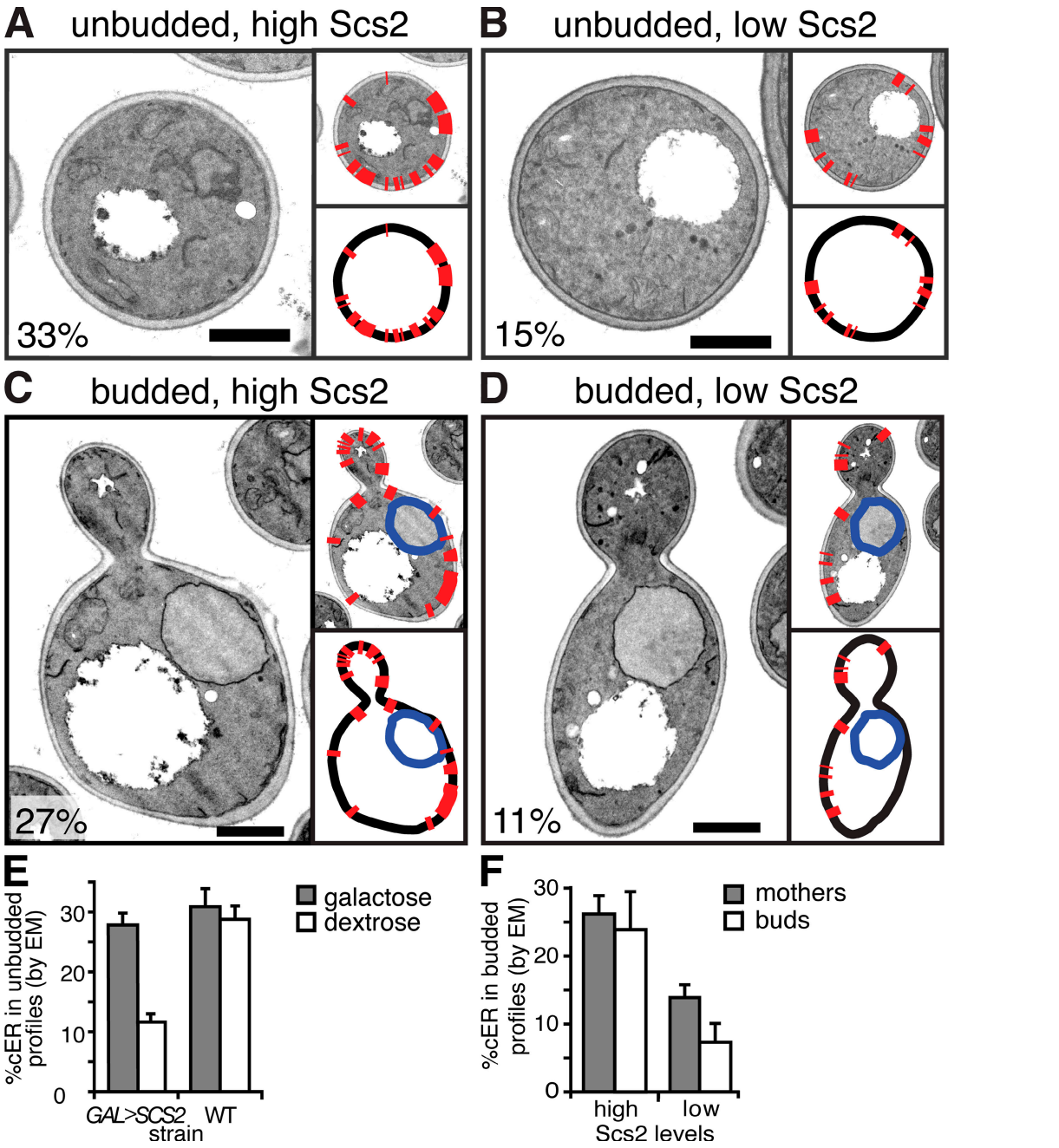

Figure 2. **Identification of cER in wild-type and *Δscs2* cells by electron microscopy.** (A–D) Electron micrographs of typical unbudded (A and B) and budding (C and D) *GAL>SCS2* (TLY251) cells grown to induce (A and C) or repress (B and D) the expression of Scs2. Electron micrographs were annotated by indicating segments of cER in red (top right), which is also shown with the whole cell outlines in black (bottom right). The proportion of cell periphery with cER is 33% (A), 15% (B), 27% (C; mother 24%, bud 35%), and 11% (D; mother 9%, bud 15%). (E) Quantitation from electron micrographs of the effect of low Scs2 on cER in unbudded cells. (left) cER in electron micrographs of *GAL>SCS2* cells (in which levels of Scs2 are high in galactose and low in dextrose). Repression of *SCS2* reduced cER to 42% of that seen with induction, which was statistically significant ($P < 10^{-7}$ by *t* test). (right) Wild-type cells (BY4742) were grown in galactose and dextrose. Amounts of cER were the same as each other ($P = 0.56$ by *t* test) and were the same as *GAL>SCS2* cells with induced *SCS2* ($P = 0.40$ and $P = 0.74$, respectively), implying that the effect on *GAL>SCS2* is specific to Scs2 and that the overexpression of Scs2 does not increase cER above wild-type levels. (F) Differential effect of low Scs2 on cER in buds and mothers. Electron micrographs of budding profiles of *GAL>SCS2* cells were quantified as in E. Low levels of Scs2 were associated with a decrease of cER: buds = 31% wild type, and mother cells = 53% wild type. Error bars indicate SEM. Bars, 1 μm.

a manner that changed throughout the cell cycle (Fig. 4, A and B). In addition, there was weak cortical targeting in some cells and targeting to the nucleolus. Targeting was stronger in cells lacking endogenous Scs2 (unpublished data), suggesting competition with endogenous Scs2 for a saturable receptor. Importantly, the same targeting was also seen with the human proteins VAP-A and -B and was not affected by the P56S mutation of VAP-B associated with amyotrophic lateral sclerosis (Fig. 4 C and not depicted; Nishimura et al., 2004). To determine whether full-length Scs2 also shows polarized targeting, we expressed GFP-Scs2

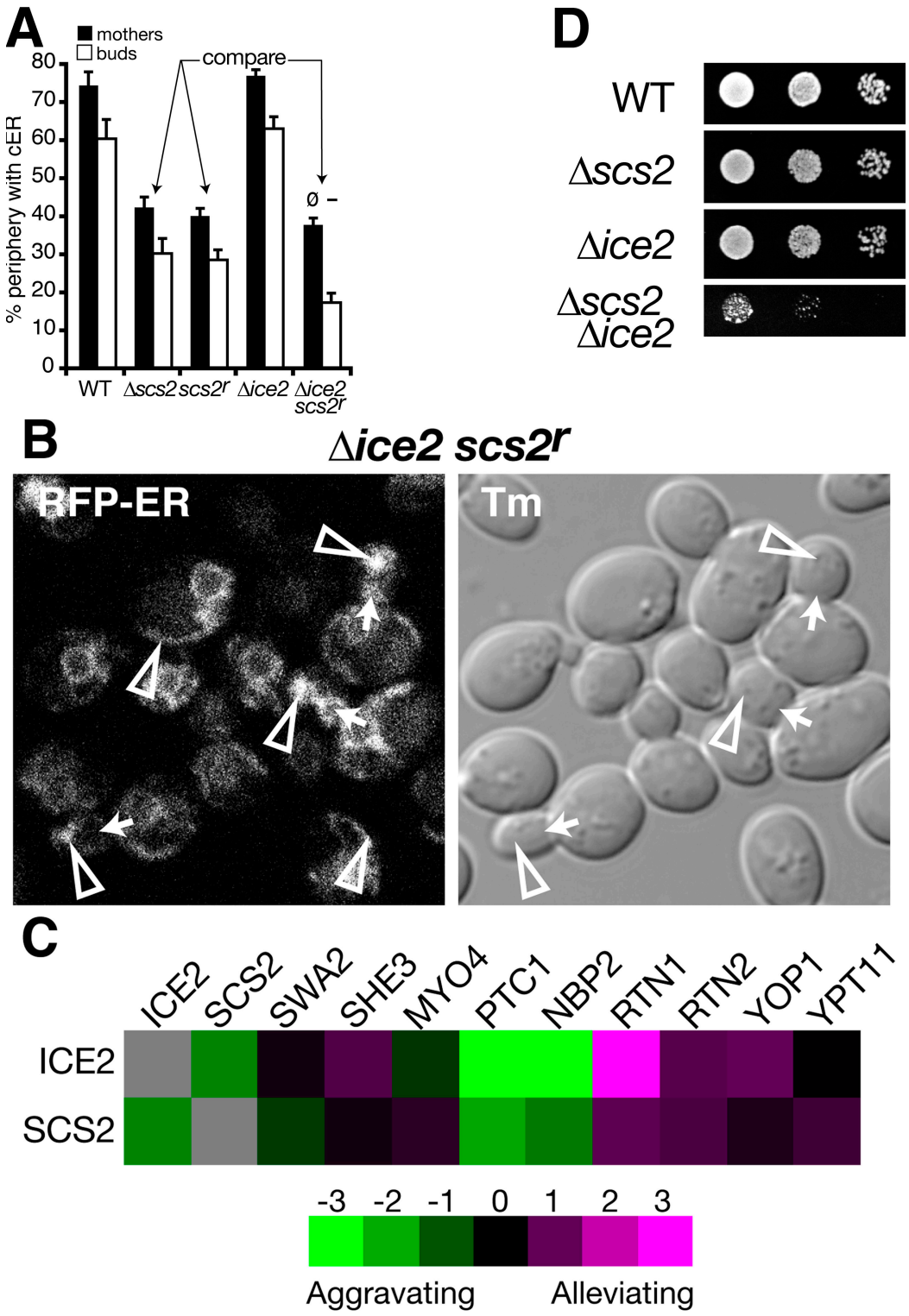

Figure 3. **Interaction of *SCS2* with *ICE2* in cER inheritance.** (A) Effect of combining mutations of *SCS2* and *Δice2*. The proportion of periphery with apposed cER in mothers (black bars) and buds (white bars) was assessed in wild-type (BY4741) yeast, strains lacking functional Scs2 (either deleted [*Δscs2*] or repressed [*scs2*^{r}]), and a double mutant strain. Compared with *Δscs2* and *scs2*^{r}, *Δice2 scs2*^{r} buds had less cER (- indicates $P \leq 0.01$ by *t* test; Ø indicates $P > 0.1$). Error bars represent SEM. (B) *Δice2 scs2*^{r} cells expressing RFP-ER, plus transmission (Tm) image. Punctate accumulations of cytoplasmic ER (arrowheads) were seen in buds but did not colocalize with bud tips. Arrows in the mothers of these cells indicate the axis of budding. (C) SGA analysis for *SCS2* and *ICE2* and genes implicated in cER inheritance. The strength of interaction is indicated by the color scale (gray, no data). (D) Growth defect of *Δscs2Δice2* cells isolated by tetrad analysis. Cells were spotted onto agar plates in 10-fold serial dilutions and grown for 2 d at 30°C on minimal medium.

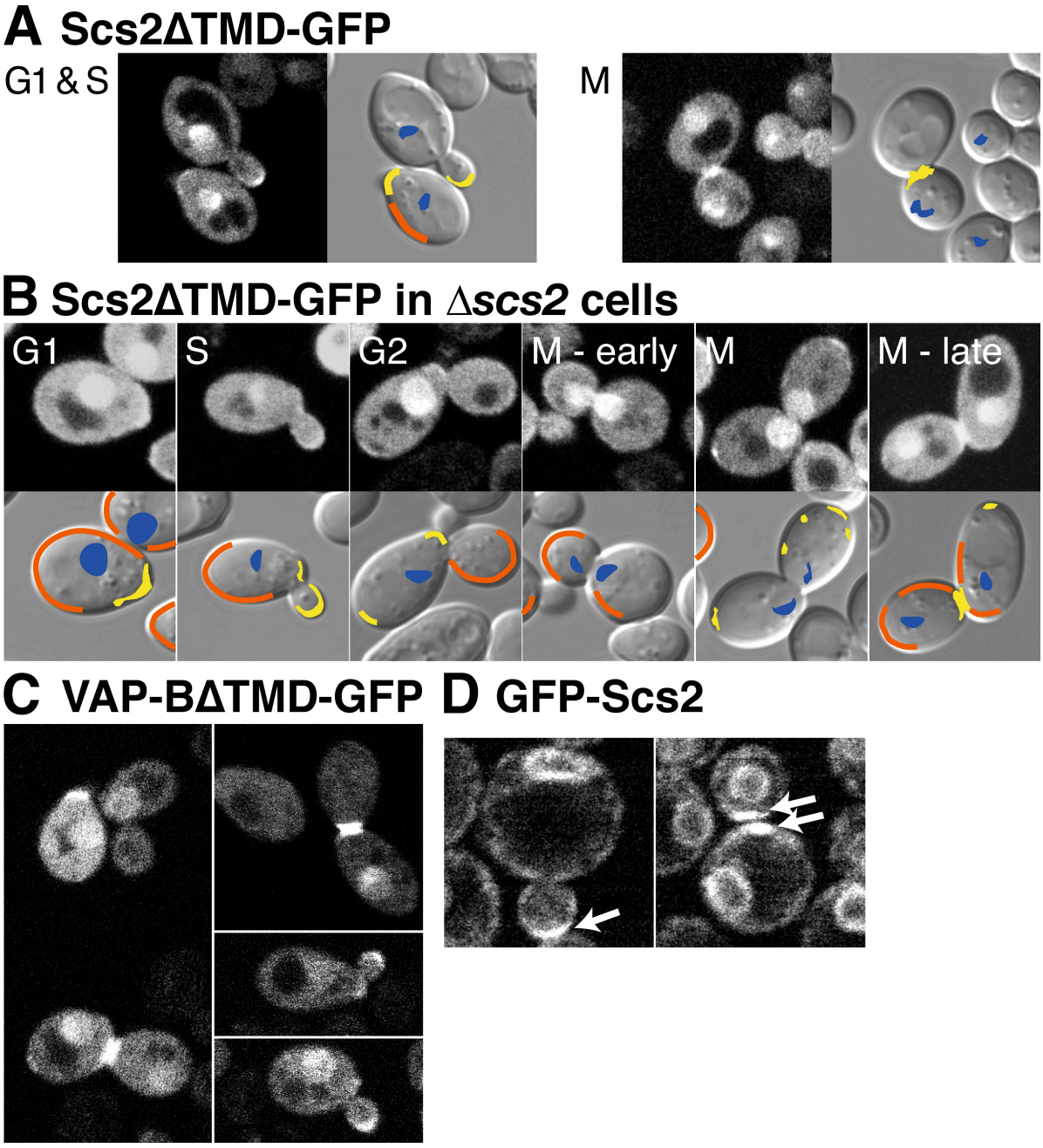

Figure 4. **Targeting by Scs2 and VAP to sites of polarized growth.** (A) Scs2ΔTMD-GFP expressed in wild-type cells. In a minority of cells, Scs2ΔTMD-GFP targets the tips of small buds (left) or sites of recent cytokinesis, likely incipient bud sites (right). The locations of targeted construct are indicated on transmission images: yellow, sites of polarized growth (bud tip and incipient bud sites); red, cortex; and blue, nucleolus, which was confirmed by costaining with a nucleolar reporter (Cgr1-RFP; not depicted). (B) A gallery of *Δscs2* cells expressing Scs2ΔTMD-GFP, with typical localizations varying with the cell cycle. Transmission images annotated as in A except yellow includes the bud neck, distal pole of mother cell, and occasional peripheral puncta. (C) A gallery of wild-type cells expressing VAP-BΔTMD-GFP. Similar targeting was shown by VAP-AΔTMD-GFP and VAP-B(P56S)ΔTMD-GFP (not depicted). (D) GFP-Scs2 (full length) expressed in wild-type cells. Arrows indicate polarized targeting.

at low levels. This revealed weak focal targeting to the tips of small buds and sites of incipient budding (Fig. 4 D). Such a minor accumulation at sites of polarized growth was not seen with other ER markers and was not seen when GFP-Scs2 was more highly expressed (unpublished data), explaining how we overlooked it previously (Loewen et al., 2003). These results show that Scs2 and other VAP homologues have a conserved interaction at sites of polarized growth.

Interaction of Scs2 at the bud tip is required for cER formation

We next studied the relationship between polarized targeting by Scs2, its role in forming cER, and the previously described interactions of Scs2. The only interaction of Scs2 to be mapped in molecular detail is with short linear FFAT motifs (two phenylalanines [FF] in an acidic tract; Loewen et al., 2003; Kaiser et al., 2005; Loewen and Levine, 2005). To test for the role of

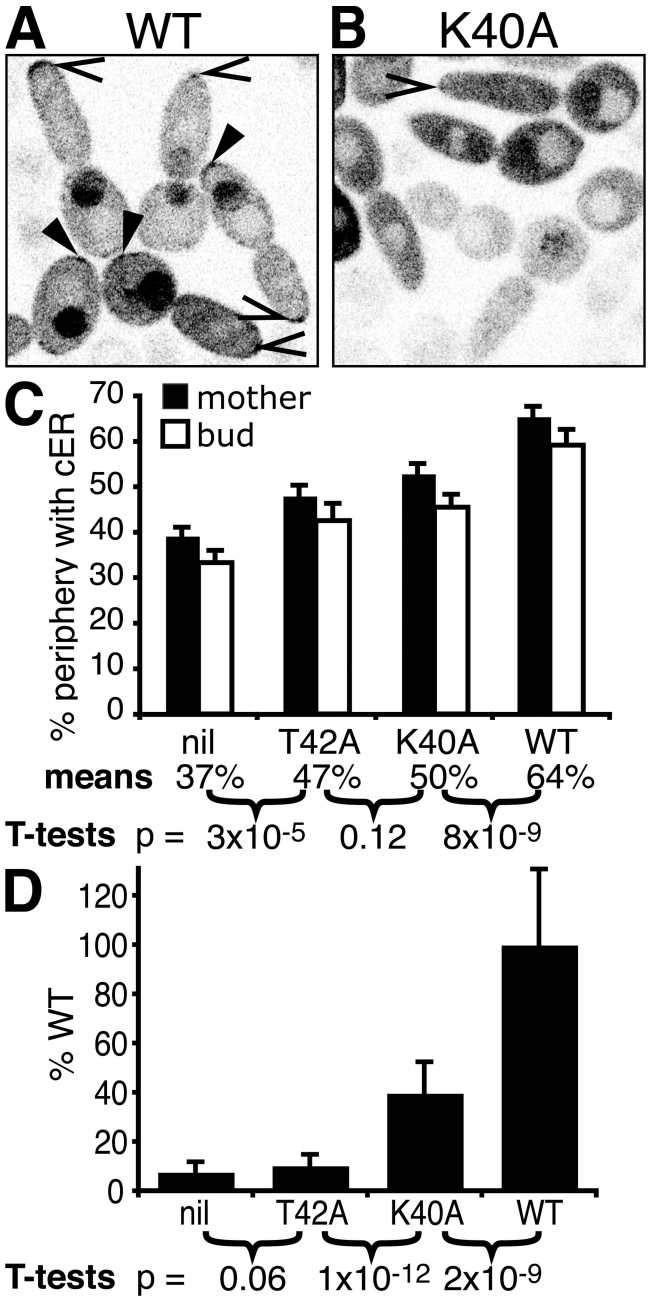

Figure 5. **Molecular determinants of Scs2 targeting and cER formation.** (A) Inverted image of *Δscs2* cells expressing Scs2ΔTMD-GFP synchronized in S phase by treatment with 300 mM HU for 4 h. Under these conditions, there is targeting to the tips of virtually all buds (open arrowheads) and the distal pole of some mothers (closed arrowheads). (B) Cells as in A expressing K40AΔTMD-GFP. Polarized targeting is almost completely lost, with a rare small area of weak targeting indicated. Nucleolar targeting is also considerably reduced, indicating that the nucleolar localization sequence is formed by the cluster of positive charges around the conserved FFAT-binding surface of Scs2 (Endo et al., 1989; Kaiser et al., 2005; Loewen and Levine, 2005). (C) The effect of mutations near the FFAT-binding site on rescue of cER by Scs2. *Δscs2* cells (CLY3 with RFP-ER integrated at *LEU2*) were transformed with an empty plasmid (nil), plasmids expressing wild-type Scs2 (WT), or mutants T42A and K40A. The proportion of cell periphery with apposed cER in mothers (black bars) and buds (white bars) was assessed. Numbers refer to the means of cER in mothers and buds together, and *t* test scores compare the effect of different plasmids. (D) Complementation of the *Δscs2Δice2* growth phenotype with variants of Scs2. Heterozygous diploid cells were transformed with the same plasmids as in C, and random spore analysis was performed to generate haploid double mutants. Rescue was quantitated by measuring colony size for at least 50 colonies per plasmid and is normalized to rescue by wild-type Scs2. Error bars indicate SEM.

Scs2–FFAT interactions, we used a panel of eight Scs2 mutants obtained from mapping the FFAT-binding site (Loewen and Levine, 2005). Within the panel, the affinity of binding to FFAT in vitro and the inhibition of Opi1 in vivo correlated perfectly with each other (Loewen and Levine, 2005). These read-outs correlated approximately with targeting of mutant ΔTMD-GFP constructs to the bud tip and septum, but there were two mutants (K40A and K84N) that targeted poorly relative to their interaction with FFAT (Table S2, available at http://www.jcb.org/cgi/content/jcb.200708205/DC1). In particular, K40A had normal FFAT binding (Loewen and Levine, 2005) and the same reversion of the ino$^-$ phenotype as wild-type Scs2 (Fig. S4 A), but K40AΔTMD-GFP localized weakly compared with wild-type Scs2ΔTMD-GFP (Fig. 5, A and B), suggesting that FFAT binding is not important for polarized targeting. Because this approach cannot completely exclude a role for FFAT, we localized Scs2ΔTMD-GFP in strains missing combinations of the four yeast proteins with FFAT motifs (Osh1, Osh2, Osh3, and Opi1) and found no defect in polarized targeting or cER structure (Table S1 and unpublished data). In addition to interacting with FFAT motifs, Scs2 has been suggested to have five FFAT-negative binding partners (Stt4, Pil1, Num1, Fks1, and Rpn10; Gavin et al., 2002), but deletion or inactivation of these, in turn, did not inhibit the polarized targeting of Scs2 (Table S1) or the formation of cER in buds (unpublished data). Overall, these results show that Scs2 has a novel, conserved interaction targeting sites of polarized growth, which might be related to its role in the formation of cER.

We next examined how mutations in Scs2 affect its function, comparing K40A (see previous paragraph) with T42A, which has no polarized targeting and does not bind FFAT (Table S2). For cER formation, both mutants rescued cER partially, K40A slightly more than T42A (Fig. 5 C). For complementation of the *Δscs2Δice2* growth defect, K40A rescued partially, and T42A was inactive (Fig. 5 D). Thus, the rescue of *Δscs2Δice2* cells correlates with cER rescue and the degree of polarized targeting but not with FFAT binding. The only other activity described for Scs2 is in gene silencing (Craven and Petes, 2001; Cuperus and Shore, 2002), which is likely related to its presence on the inner nuclear envelope (Brickner and Walter, 2004). We excluded a role for this pool of Scs2 in cER inheritance by comparing the activities of intranuclear and extranuclear variants of Scs2: the rescue of cER was greater with extranuclear Scs2 (Fig. S4, B and C). Together, these data suggest that Scs2 has a novel interaction at sites of polarized growth that is required for cER formation and the rescue of *Δscs2Δice2* cells.

Polarized targeting of Scs2 is mediated by the polarisome

Targeting of Scs2 to the bud tip might reflect either active delivery by an actin-mediated process with continuous recycling (Ayscough et al., 1997) or binding to a more static bud tip component.

We tested this by depolymerizing actin with a latrunculin A treatment for 20 min, which had no effect on Scs2ΔTMD-GFP targeting but did delocalize Sac6-RFP (unpublished data). Similarly, inhibition of membrane fusion in a *sec18-1* strain did not affect targeting (unpublished data). This suggests that the receptor for Scs2 at the bud tip is not rapidly cycling (for example, on secretory vesicles; Roumanie et al., 2005). Longer treatment with latrunculin A (60 min) did reduce targeting, suggesting that the receptor for Scs2 is not completely static (a property of many bud tip components; Ayscough et al., 1997).

We next used a candidate approach to look for the receptor for Scs2 at sites of polarized growth. 57 deletion strains missing known bud tip proteins were tested for targeting of Scs2ΔTMD-GFP, but in all of these strains there was at least some polarized localization, indicating that none of the genes tested code for the sole Scs2 receptor (Table S1). 10 of the deletion strains showed variant targeting: two were better localized than wild type (*Δbim1* and *Δrom2*), five were less well localized (*Δbem2*, *Δbem3*, *Δbni1*, *Δpea2*, and *Δspa2*), and three had punctate Scs2ΔTMD-GFP at the bud tip (*Δaxl2*, *Δbud3*, and *Δbud6*). The clearest conclusion from this is that targeting requires the polarisome, which is a 12S complex of Bni1, Bud6, Pea2, and Spa2 that establishes polarity in yeast (Sheu et al., 1998; Pruyne and Bretscher, 2000). Interestingly, some of these components are also partially mobilized by long-term treatment with latrunculin A (Ayscough et al., 1997). To confirm that Scs2 targeting is mediated by the polarisome, we compared the distributions of RFP-Scs2ΔTMD and GFP-tagged Pea2 and found that the two proteins were superimposed or closely adjacent (Fig. 6 A). Among the candidates for Scs2 receptors that we excluded were Sho1 (the yeast homologue of occludin, which binds VAP; Lapierre et al., 1999) and the known polarisome interactors Msb3/Msb4 and Sph1 (tested in a *Δspa2* strain; Table S1; Arkowitz and Lowe, 1997; Sekiya-Kawasaki et al., 2002). These data suggest that the receptor for Scs2 is a currently undefined bud tip component acting downstream of the polarisome.

The polarisome cooperates with Scs2 in attaching cER to bud tips

If the polarisome is important in targeting Scs2, there might be cER abnormalities in polarisome mutants. Using our fluorescent reporter, we found that *Δspa2*, *Δpea2*, and *Δbud6* cells had normal ER architecture (unpublished data), indicating that the modest delocalization of Scs2ΔTM-GFP in these mutants does not affect cER inheritance. In contrast, cER in *Δbni1* buds was abnormal, often failing to reach the bud tip (Fig. 6 B). Instead, cER formed a cup shape around the bud neck, a unique phenotype suggesting that Bni1 affects more than just Scs2 targeting. This can be understood in light of previous findings that Bni1 is required for the assembly of actin cables in the bud (Evangelista et al., 2002), which are used by Myo4 to transport ER (Estrada et al., 2003). We next examined the effect on cER of combining *Δscs2* with the deletion of polarisome components. *Δpea2Δscs2* cells and *Δspa2Δscs2* cells both showed cER defects similar to *Δscs2* cells (Figs. 6 C and S3 C). *Δbud6Δscs2* cells showed an additional phenotype, with multiple cytoplasmic ER tubules originating from the bud neck and very little cER at the bud tip (Fig. 6 D). *Δbni1Δscs2* cells showed a phenotype similar to but far stronger than *Δbni1* cells, with cER absent from most bud tips and cup-shaped cER emanating from the bud neck not only in buds but also in many mother cells (Fig. 6 E). Videos show cER creeping through the bud neck and along the cell cortex into the proximal bud (Videos 1 and 2, available at http://www.jcb.org/cgi/content/full/jcb.200708205/DC1), with no cytoplasmic ER tubules crossing to the bud tip as in wild-type cells (Fehrenbacher et al., 2002; Du et al., 2006). Because Bni1 is only partially responsible for targeting Scs2 to the bud tip, the stronger phenotype of *Δbni1Δscs2* cells suggests that *Δscs2* is epistatic to *Δbni1*. If Bni1 (and its role in the polarisome) cooperates with Scs2 in attaching cER to the bud tip, the polarisome functions in a pathway parallel to *ICE2* and should show genetic interactions with *ICE2* but not with *SCS2*. Indeed, SGA analysis showed that *ICE2* (but not *SCS2*) has strong aggravating genetic interactions with *BNI1*, *BUD6*, and *SPA2* (Fig. 6 F). Therefore, in the absence of Ice2, recruitment of ER to the bud tip by the polarisome becomes essential.

Lack of Scs2 causes cellular elongation

Δscs2 mutants have been reported as one of the most elongated yeast deletion strains, their elongation putting them in the 99th centile of 4,800 strains measured in a genome-wide study of cell shape (Saito et al., 2004). We found the same elongation in *Δscs2* mutants of both BY4741 (Fig. 7, A and B) and RS453B strains with deleted or repressed *SCS2* (not depicted). We tested which aspects of the Scs2 protein are important for rescue of cell shape. First, there was no restoration of cell shape if Scs2 was either made soluble by deleting its TMD or if full-length Scs2 was retained on the inner nuclear membrane (Fig. S4 D), indicating that Scs2 needs to be anchored in the extranuclear ER to rescue cell shape. Second, K40A and T42A mutants both partially rescued cell shape, although slightly more so for K40A (Fig. 7 C). Finally, the known interactors of Scs2 (Opi1, Osh1/Osh2/Osh3 [singly and together], Fks1, Num1, Pil1, Rpn10, and Stt4) were not important in cell shape, as the lack of any of these proteins did not cause elongation (unpublished data). Thus, rescue of elongation appeared to correlate with the factors we found to be required both for polarized targeting of Scs2ΔTMD and for cER formation, suggesting that cellular elongation results from defective cER inheritance. Although this link has not been reported previously, *Δice2*, *Δshe3*, *Δypt11*, *Δrtn1*, and *Δrtn2* strains are elongated (albeit less than *Δscs2*), whereas *Δmyo4* and *Δswa2* have normal shape and *Δptc1* and *Δnbp2* are among the most rounded of all strains, similar to *Δsec3* (Wiederkehr et al., 2003; Saito et al., 2004; and unpublished data). Thus, although all genes implicated in cER inheritance and structure do not appear to act similarly, cellular elongation is a common feature.

Defective cER inheritance activates Swe1

The morphogenesis checkpoint results from an imbalance between Swe1 and Mih1 (a Cdc25 homologue), which respectively inhibit and activate Clb2–Cdc28 complexes that control the apical isotropic growth switch in G2 (McMillan et al., 1998; Longtine et al., 2000; Lew, 2003). Overactivation of Swe1 delays the switch, leading to cellular elongation; in contrast,

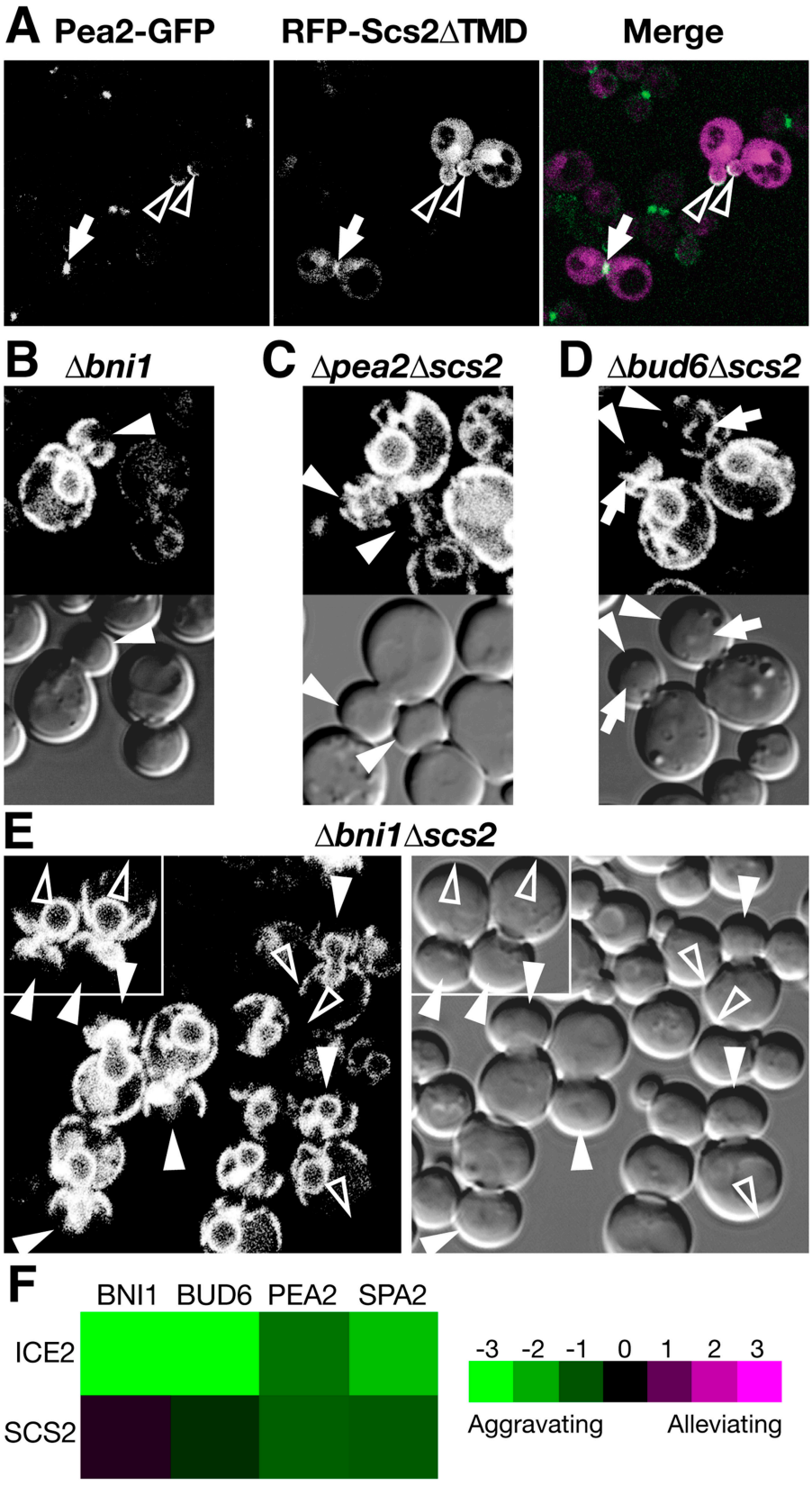

Figure 6. **Role of polarisome in targeting Scs2 to sites of polarized growth.** (A) Colocalization of Pea2-GFP with RFP-Scs2ΔTMD. Single images are shown together with a merged image in which GFP and RFP are colored green and purple, respectively, with colocalization (white) at bud tips (arrowheads) and a site of recent cytokinesis (arrows). (B–E) ER in polarisome mutants visualized using RFP-ER: *Δbni1* (B), *Δpea2Δscs2* (C), *Δbud6Δscs2* (D), and *Δbni1Δscs2* (E). Transmission images are also shown. In all of B–E, cortical regions of buds lack cER (closed arrowheads). Associated with *Δbni1* (B and E), cER is missing from bud tips; cER is also absent from distal poles of *Δbni1Δscs2* mother cells (open arrowheads placed in mother cells; E). *Δbud6Δscs2* buds also contain excess strands of cytoplasmic ER (arrows; D). (F) SGA analysis identifies aggravating interactions between *ICE2* and components of the polarisome.

deleting *SWE1* hastens the switch, producing rounder cells. The *Δscs2* strain was significantly rounded up by the introduction of *Δswe1* (Fig. 8 A), indicating that the effect of *Δscs2* on cell shape is caused by an imbalance between Swe1 and Mih1. In contrast, the milder elongation of *Δice2* was not reverted in *Δice2Δswe1* cells. To confirm the suggestion that Swe1 overactivity is responsible for shape changes in the *Δscs2* strain, we determined the effect on shape of overexpressing Hsl7, an

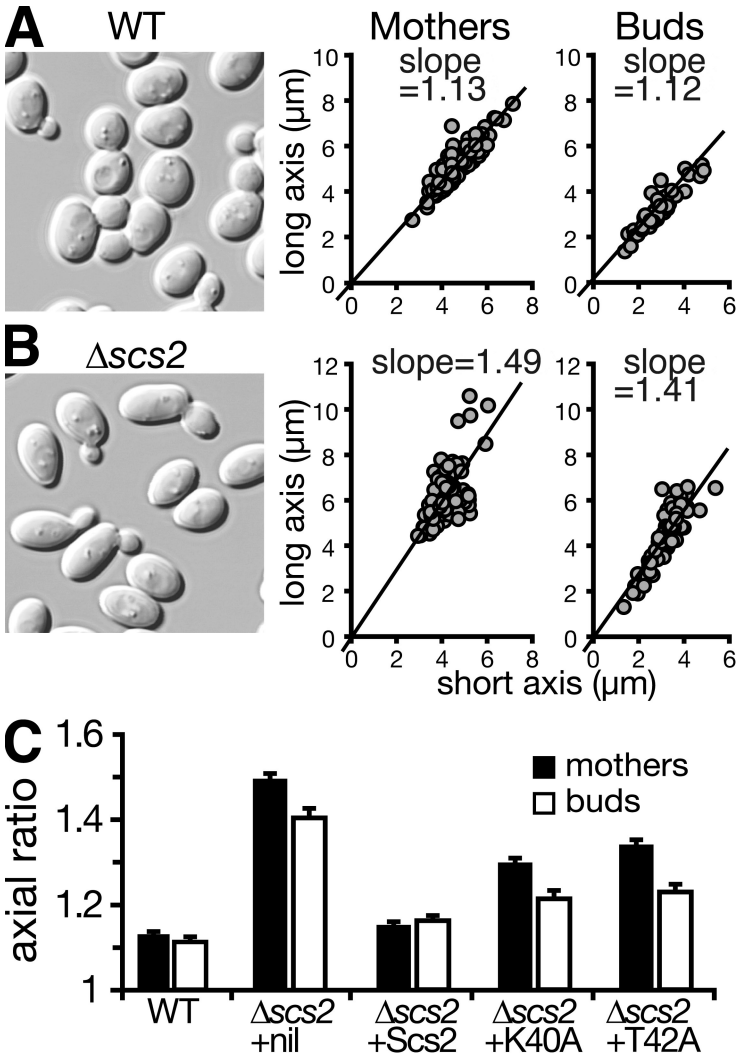

Figure 7. ***Δscs2* cells are elongated.** (A and B) Cell shape of wild-type (WT; A) and *Δscs2* cells (B). Transmission images of fields of cells were processed as described in Materials and methods to measure cell length and width, here plotted for mother cells and daughters separately, together with lines of best fit. (C) The axial ratios (length/width) were calculated for mother cells and buds of wild-type and *Δscs2* strains carrying a plasmid, either empty or with Scs2, wild-type, or K40A or T42A mutants. The elongation of buds correlated with but was less than elongation in mothers. Error bars represent SEM.

adaptor protein that brings Swe1 to the septin ring to facilitate its phosphorylation by Hsl1 and subsequent degradation (Fig. 8 B; McMillan et al., 1999; Shulewitz et al., 1999). Excess Hsl7 considerably rounded up the *Δscs2* strain, indicating that its elongation is caused by excess Swe1 activity.

Because these results indicate increased Swe1 activity in *Δscs2* cells, we investigated Swe1 levels. We found that levels of Swe1-myc were increased in both *Δscs2* and *Δice2* strains, either in unsynchronized cells (Fig. 8 C) or in cells synchronized in S phase by incubation with hydroxyurea (HU; Fig. 8 D). When samples from cells with HU were separated on gels without SDS to exaggerate the retarding effect of hyperphosphorylation (Fig. 8 E; Sakchaisri et al., 2004; Harvey et al., 2005), we found that phosphorylation of Swe1-myc was affected by *Δscs2* and *Δice2*. Both mutations caused an increase in partially hyperphosphorylated Swe1-myc (Fig. 8 E, lanes b and c), the most active species, and a lack of the smear of maximally hyperphosphorylated Swe1-myc (found in wild-type cells; Fig. 8 E, lane a), which is less active and is the substrate for ubiquitination and degradation (Harvey et al., 2005). Alongside the changes in phosphorylation, myc-positive degradation products appeared in both *Δscs2* and *Δice2* strains (Fig. 8 D), indicating altered degradation. These results demonstrate that loss of both *SCS2* and *ICE2* leads to increased Swe1 activity even though we found that the inactivation of Swe1 rescues the shape of *Δscs2* only, not *Δice2*.

We next tested the effect of *SWE1* loss on the viability of strains with defective cER (Fig. 8 F). The deletion of *SWE1* in a wild-type background slightly increased the growth rate as reported previously (Harvey and Kellogg, 2003). The deletion of *SCS2* did not affect the growth rate, nor did deletion of *SWE1* in the *Δscs2* strain, indicating that the main effect of *SWE1* in *Δscs2* cells is on shape. The deletion of *ICE2* resulted in a mild growth defect that was considerably exacerbated by the deletion of *SWE1*. However, the loss of *SWE1* in *Δscs2Δice2* cells, which led to considerable rounding up (axial ratio of 1.18 compared with 1.41 in *Δscs2Δice2* cells), strongly impaired growth (doubling time of 385 min compared with 128 min), indicating that the loss of cER renders cells dependent on Swe1 for cell survival, with *Δscs2* having an additive effect beyond *Δice2* alone.

Loss of Scs2 or Ice2 affects septin organization

Many pathways increase Swe1 activity. One is ER stress, which causes cell death in the absence of signals through Mpk1 in the

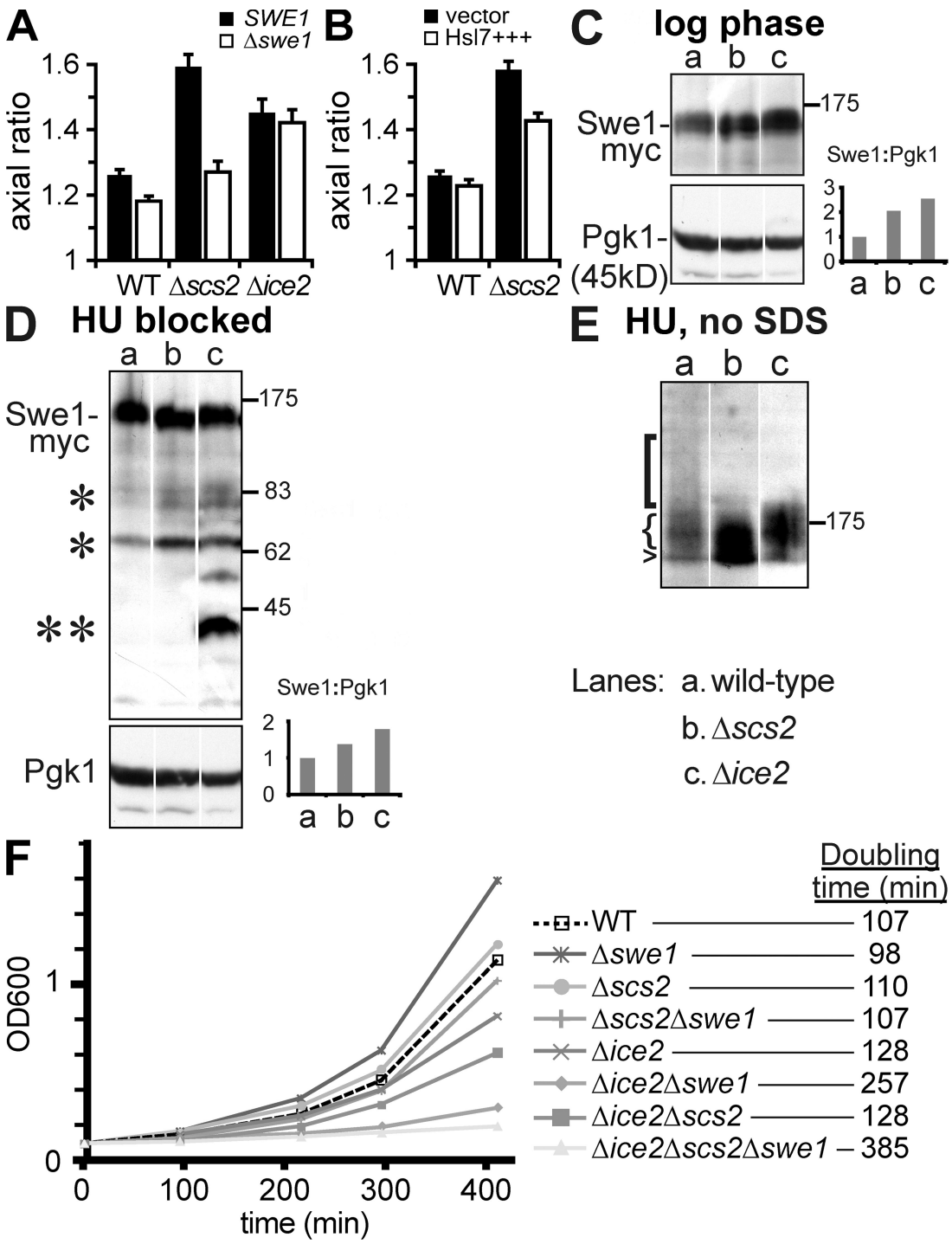

Figure 8. **Interaction of *SCS2* and *ICE2* with *SWE1*.** (A) Axial ratios of wild-type, *Δscs2*, and *Δice2* cells compared with their *Δswe1* counterparts. *Δswe1* led to statistically significant rounding up for wild type ($P = 0.0002$ by *t* test) and *Δscs2* ($P < 10^{-8}$ by *t* test) but not for *Δice2*. (B) Axial ratios of wild-type and *Δscs2* cells compared with the same strains overexpressing Hsl7 from the *GAL1/10* promoter. Error bars represent SEM. (C) Cell lysates from log-phase cultures of wild-type, *Δscs2*, and *Δice2* strains in which the genomic copy of Swe1 was tagged with a 12x myc cassette were separated on SDS-PAGE gels and immunoblotted for c-myc. Equal loading of samples was ensured by blotting for phosphoglycerokinase (Pgk1). The main full-length Swe1-myc band was quantified relative to Pgk1. (D) The same yeast strains were treated with HU for 4 h and analyzed for total Swe1-myc content as in C. Asterisks indicate major reproducible breakdown products. (E) Analysis of Swe1-myc in HU-treated samples from D on polyacrylamide gels without SDS. The different forms of Swe1-myc indicated are fastest migrating (arrowhead), partially hyperphosphorylated slower migrating forms (curly bracket), and smear of maximally hyperphosphorylated forms rising above that in lane a (square bracket; Harvey et al., 2005). Blots are from a single representative of three similar experiments. In C–E., molecular weights are indicated, and Pgk1 migrates at 44 kD. (F) The effect of deleting *SWE1* on growth rates and doubling times of wild-type, *Δscs2*, *Δice2*, and *Δscs2Δice2* strains assayed in rich medium as described in Materials and methods.

MAPK to calcineurin pathway (Bonilla and Cunningham, 2003). Because *MPK1* was not essential for cell survival in *Δscs2* or *Δice2* strains (unpublished data), it appears that cER inheritance defects do not activate this ER stress pathway. Two defects in the cytoskeleton of the bud signal to Swe1 via the morphogenesis checkpoint: perturbed actin and septins (Lew, 2003). For actin, one pathway following its depolymerization signals via Mpk1 to inhibit Mih1, leaving Swe1 unopposed (Harrison et al., 2001). However, the combination of *Δmpk1* with *Δscs2* or *Δice2* did not reduce elongation, nor did the overexpression of Mih1 (unpublished data), implying that *Δscs2* and *Δice2* do not require Mpk1 for the elongation. Actin defects may also activate the high osmolarity glycerol pathway, which lies upstream of Swe1 activation by delocalizing Hsl7 (Clotet et al., 2006). However, Hsl7-GFP was not delocalized in *Δscs2* and *Δice2* strains (unpublished data), suggesting that the high osmolarity glycerol pathway is not activated by cER defects.

Septin disorganization results in budding defects, bud neck deformities, and an increase in Swe1 levels (Lew, 2003). Therefore, we looked for signs of altered septin organization in *Δscs2* and *Δice2* cells and found that a small minority had multiple buds compared with this being undetectable in wild-type cells (Fig. 9 A). This led us to look for the same phenotype in the *Δscs2Δice2* strain, in which >40% of cells had multiple buds, indicative of septin defects. To directly visualize septins, we used a GFP-tagged version of the septin Cdc10. *Δscs2Δice2* cells formed defective septin rings and mislocalized Cdc10-GFP mainly to bud tips, phenotypes that were rare in single mutants but completely absent in wild-type cells (Fig. 9, A and B). We also performed SGA analysis of *SCS2* and *ICE2* with bud neck kinases that affect septin function, which identified interactions of both *SCS2* and *ICE2* with *CLA4*, a key kinase in septin ring assembly (Longtine et al., 2000; Schmidt et al., 2003; Kadota et al., 2004; Versele and Thorner, 2004), and also between *SCS2* and *HSL1* (Fig. 9 C). This is evidence for the specific involvement of cER in septin assembly. We confirmed the interactions with *CLA4* by tetrad analysis (Fig. 9 D) and examined septin assembly in the double mutants. *Δcla4* considerably disrupted septins (Fig. 9, A and B), an effect intensified in both *Δscs2Δcla4* and *Δice2Δcla4*, particularly leading to chains of unseparated cells (Fig. 9 B) that were multinucleate (not depicted). In some cases, septin collars were completely absent or present only as puncta at the erstwhile bud neck (Fig. 9 B). The cellular phenotype of the double mutants suggests the improper assembly of septin collars, leading to a failure in the completion of cytokinesis, and explains the growth defects.

Discussion

In this study, we find that the ER transmembrane protein Scs2 is required for cER inheritance. Scs2 appears to act in the attachment phase, as ER tubules lacking Scs2 are delivered into buds but not to bud tips. Scs2 interacts with an unidentified bud tip component, suggesting that it bridges directly from the ER to the plasma membrane. Bud tip targeting of Scs2ΔTMD is not indirect via another component of cER because it occurs where cER is absent from the bud tip (unpublished data). We propose that bridging by Scs2 acts at a similar stage in cER inheritance as the translocon–exocyst interaction, although with some differences. Loss of translocon components had no discernible effects on cER inheritance in our strains (unpublished data), and, in other studies, the loss of exocyst components does not affect cER in mother cells (Wiederkehr et al., 2003; Reinke et al., 2004), which is considerably reduced in cells lacking Scs2.

SCS2 showed aggravating genetic interactions with *ICE2*, whose protein product is also integral to the ER and, when deleted, results in cER defects in buds and mothers. The variation of the growth phenotype of *Δscs2Δice2* with medium is opposite to that reported previously for *Δsec3* mutants, which fair worse on rich medium (Du et al., 2006), and in neither case is the reason yet understood. As one might predict, mutations of the polarisome, which lies upstream of Scs2 targeting, also show aggravating genetic interactions with *Δice2*, although we cannot exclude the possibility that these interactions involve regulation of the exocyst by the polarisome. The alleviating interaction between *Δice2* and reticulons, especially *Δrtn1*, might result from the conversion of cER into large sheets caused by the loss of Rtn1 (and Rtn2 less so; De Craene et al., 2006; Voeltz et al., 2006), thus reversing the effect of mutations that decrease cER. Together, the genetic interactions and the extreme loss of cER in *Δscs2Δice2* cells imply that Scs2 and Ice2 function in parallel or partially redundant pathways attaching ER to the cortex.

The involvement of the polarisome in Scs2ΔTMD targeting led to the finding that Bni1 is required for ER tubule movement in buds, a defect greatly exaggerated in *Δscs2Δbni1*, where cER also failed to reach the distal pole of mother cells. The effects of losing Bni1 might be predicted from its function in nucleating actin filaments at bud tips and the presence of some Bni1 at the distal pole of mothers (Evangelista et al., 2003; Matheos et al., 2004). The slow movement of cER through the bud neck in *Δscs2Δbni1* cells is reminiscent of the actin-dependent short-range dynamic reorganization of cER reported in both yeast and higher eukaryotic cells (Prinz et al., 2000; Poteryaev et al., 2005). This is a compensatory mechanism by which buds receive cER, which was hypothesized to exist previously (Estrada et al., 2003). Because Scs2 and Bni1 function in the preferred long-distance pathway of cER inheritance, the genetic interactions of *Δice2* with both *Δscs2* and *Δbni1* suggest that Ice2 acts in this second pathway.

The finding that two genes involved in cER inheritance are also required for septin assembly indicates that there is a causal link, although the molecular basis remains unknown. Septins form filamentous scaffolds for various cellular functions, act as diffusion barriers, and rearrange in cellular events such as cytokinesis (Spiliotis and Nelson, 2006). Within the bud neck, the septin ring and cER both interact with the cortex, and they also interact with each other, as septins were recently shown to create a diffusion barrier in cER at the bud neck (Luedeke et al., 2005). During budding, not only does the ER have to rearrange but the septin ring grows into the bud to form an hourglass that then splits into two rings (Longtine and Bi, 2003). Therefore, it is possible that the effects of defective cER inheritance on septins result from local interactions with altered ER at the bud neck. However, because we found no gross alteration in

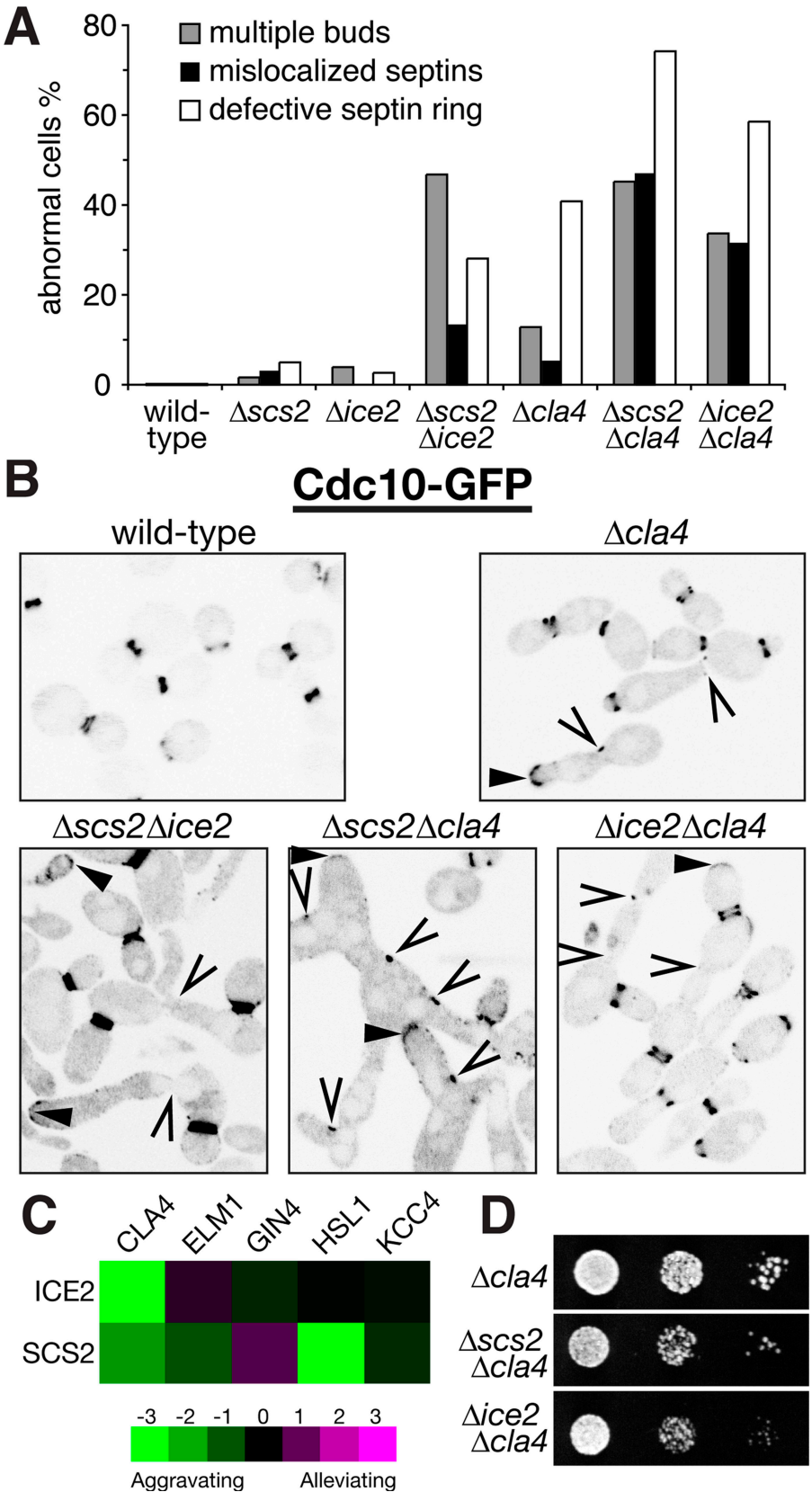

Figure 9. **The effects of *Δscs2* and *Δice2* on organization of the septin Cdc10.** (A) Quantification of septin localization, assembly, and multibudded phenotype in mutant strains with the endogenous septin Cdc10 tagged with GFP. Strains were grown overnight in rich medium and diluted back into minimal medium for 8 h. Over 100 cells were counted for each strain, and results are plotted as the percentage of abnormal cells. (B) Distribution of Cdc10-GFP in wild-type, *Δcla4*, *Δscs2Δice2*, *Δscs2Δcla4*, and *Δice2Δcla4* strains from A. Note the mislocalized septins usually found at bud tips (closed arrowheads) and defective or absent septin rings (open arrowheads). (C) Results of SGA analysis for *ICE2* and *SCS2* with bud neck kinases that affect septin function. (D) Growth defect of *Δscs2Δcla4* and *Δice2Δcla4* strains isolated by tetrad analysis, assayed as in Fig. 3 D.

ER morphology at the bud neck (it does not accumulate there, for example), we favor the possibility that a feature of ER within buds regulates septins. Normal bud cER may function to promote septin assembly, and it is also possible that excess cytoplasmic ER in buds impairs septin organization. Relevant cER functions include the recruitment of specific septin regulators

(for example, Cdc28 is found on the ER; Harvey et al., 2005; Verges et al., 2007), or, alternatively, the influence may be indirect via a generic function of cER. No specific essential function has been ascribed to cER rather than cytoplasmic ER, but apposition of ER to the bud plasma membrane allows the direct, nonvesicular traffic of lipids, calcium, and even proteins (Pichler et al., 2001; Berridge, 2004; Juschke et al., 2004).

Because septins scaffold multiple kinases that phosphorylate Swe1, the bud neck is the physical location where many cellular inputs are integrated to regulate G2→M progression (Keaton and Lew, 2006). This close interrelationship means that even a minor defect in septin architecture is amplified by the activation of Swe1, which, in turn, inhibits septin accumulation at the bud neck (Gladfelter et al., 2005). Thus, the abnormalities in septin assembly seen in *Δscs2* and *Δice2* mutants, the first reported for any primary defect in the ER, may be subtle (Fig. 9 A), but they are also functionally important, as shown both by synergy with the deletion of *CLA4* (a regulator of septins and Swe1) and by the strong synthetic effect in the double *Δscs2Δice2* mutant. cER inheritance has properties of a classic checkpoint in that overriding the checkpoint is strongly detrimental to growth (Fig. 8 F). In *Δscs2Δice2Δswe1* cells, the switch from apical to isotropic growth occurs, but cells are then very slow to divide. In comparison, the activation of Swe1 in *Δscs2Δice* cells aids growth, presumably by allowing the bud extra time to acquire ER before actin depolarizes, even though cortical attachment is slow thereafter.

cER distribution is now the second example in which the nuclear cell cycle machinery responds to the distribution of extranuclear membranes, in addition to breakdown of the Golgi ribbon in higher eukaryotic cells in transit through G2/M (Sutterlin et al., 2002). Given the precise way in which organelles are arranged in individual cell types, it is not entirely surprising that cells have adapted to monitor their distribution. Although our results focus on VAP in yeast, the identical polarized targeting of human VAP-A/B suggests that VAP plays a part in polarized functions of the ER in higher eukaryotic cells. Among the most polarized cell types are neurons, which have highly asymmetric processes containing specialized subdomains of ER (Rolls et al., 2002; Mironov and Symonchuk, 2006). The position of this ER, both pre- and postsynaptically, generates signals detected locally (Collin et al., 2005; Bardo et al., 2006; Mironov and Symonchuk, 2006), and it is possible that these signals also reach the nucleus. The relevance of VAP in this process is underlined by the finding that mutations in human VAP-B cause motor neuron disease (Nishimura et al., 2004).

Materials and methods

Plasmids

All plasmids were based on the pRS series and contained the constitutive portion of the *PHO5* promoter except when indicated. Plasmids used to visualize ER in living cells by confocal microscopy were as follows: (1) the TMD of Scs2 (residues 220–244; sequence ENESSSMGIFILVALLILVLGWFYR) placed after the tandem repeat of dimeric dsRed (RFP-ER) cloned into pRS416 (*CEN URA3*) or pRS405 (*LEU2*; because of its minimal size [25 amino acids], this targeting motif minimizes the possible effect of the septin-mediated diffusion barrier at the bud neck [Luedeke et al., 2005]; (2) the C terminus of Sec12, including its TMD (residues 355–471) after GFP cloned into pRS406 (*URA3*; gift of H. Pelham, Laboratory of Molecular Biology, Cambridge, UK; Sato et al., 1996); (3) and the sterol ester synthase Are2 tagged with GFP (gift of G. Daum, Technical University Graz, Graz, Austria; Zweytick et al., 2000). For simultaneous visualization of ER and plasma membrane by confocal microscopy, both RFP (RFP-ER) and a plasma membrane–targeting reporter, Psr1(N-term) (residues 1–28; MGFISSILCCSSETTQSNSNSAYRQQQS; Siniossoglou et al., 2000), followed by GFP were cloned into the vector YCp50 (*CEN URA3*). Plasmids used in Scs2 rescue experiments, including K40A and T42A mutants, were previously described (Loewen and Levine, 2005) based on pRS416 and include a myc tag (MEQKLISEEDL) before the Scs2 sequence. The plasmid Scs2-Prm3 is similar to the rescue plasmids, but, after residue 219 of Scs2, the TMD is replaced by the C-terminal 65 residues of Prm3 (69–133). The plasmid Scs2-Prm3ΔNLS omits the NLS of Prm3 (i.e., residues 74–133; Beilharz et al., 2003). GFP-Scs2-Prm3 plasmids are constructed similarly with GFP at the N terminus of the myc tag. Plasmids expressing Scs2ΔTMD-GFP and variants were based on pRS416 and contain the coding region of Scs2 missing the TMD (1–224 + linker RGAGAGAPVEK) followed by GFP. VAP-BΔTMD-GFP is the same but contains the human VAP-B cytoplasmic domain (1–222 + linker PVEK). Plasmid RFP-Scs2ΔTMD contains dimeric RFP and residues 1–225 of Scs2 in pRS416. YCpLG-GFP-HSL7 (gift of J. Thorner; University of California, Berkeley, Berkeley, CA) expresses GFP-tagged Hsl7 from the *GAL1/10* promoter (Shulewitz et al., 1999). Induction to examine Hsl7 localization was for 90 min in minimal medium, and induction for the effect of Hsl7 on cell shape was for 8 h. Plasmid DLB2258 (gift from D. Lew; Duke University Medical Center, Durham, NC) is derived from pJM1102 (McMillan et al., 2002) and integrates at the *SWE1* locus to introduce a 12-myc cassette after the Swe1 coding region without generating an untagged adjacent copy. Overexpression of C terminal–tagged Mih1 was achieved from a 2μ plasmid containing the *GAL1* promoter (Open Biosystems) and was checked by Western blotting.

Strains

Deletion strains were obtained from freezer stocks of the yeast deletion collection (BY4741, Mat a, and KanMX) unless otherwise stated. Other gene deletions were constructed by the PCR method with the heterologous markers *Schizosaccharomyces pombe HIS5*, *Kluyveromyces lactis URA3*, or NatR. Strain CLY3 is a *Δscs2-HIS5 S. pombe* derivative of the wild-type strain RS453B (Levine and Munro, 2001). TLY251 is a strain with the inducible expression of Scs2 achieved by replacing the *SCS2* promoter with the inducible/repressible *GAL1/10* promoter, as previously reported (Loewen et al., 2003). Repressible *SCS2* was also introduced into *Δice2*. These strains were grown either in galactose for the induction of *SCS2* or switched to dextrose for >16 h to repress *SCS2* function (*scs2*^{r}; Loewen et al., 2003, 2004). Double deletion strains with *SCS2* and *ICE2* were constructed by replacement of the *SCS2* ORF with *S. pombe HIS5* in the corresponding single-deletion strains based on BY4741. *SCS2* and *ICE2* single- and double-deletion strains as well as all *Δswe1* and *Δcla4* derivatives were also derived from the meiotic products of heterozygous diploids, with multiple spores of each genotype being compared. The *Δsbh1Δsbh2* strain was made by replacement of the *SBH2* ORF with *S. pombe HIS5* in *Δsbh1*. A strain dependent on a conditional allele of *STT4* has been described previously (Levine and Munro, 2002). *Δfks1Δfks2 fks1-1154*^{ts}, *sec18-1*^{ts}, *Δmsb3Δmsb4*, and *Δspa2Δsph1* strains were gifts from Y. Ohya (University of Tokyo, Tokyo, Japan), H. Pelham, E. Bi (University of Pennsylvania School of Medicine, Philadelphia, PA), and R. Arkowitz (Universite de Nice, Nice, France). In each experiment, comparable wild-type parental strains were included. To test the function of temperature-sensitive alleles, mutant and parent cells were grown at 25°C and transferred to 37°C for 30 min before visualization. Strains isogenic to BY4741 expressing Pea2-GFP and Cdc10-GFP were purchased from Invitrogen. Mutant strains with Cdc10-GFP were made by mating with deletion strains in the same background and sporulation. Growth assays were performed on isogenic strains made by mating and tetrad analysis. For quantitation of doubling times, cultures were diluted to OD_{600} = 0.1 and assayed over 7 h. Because *Δscs2Δice2* strains and derivatives showed strong cell shape phenotypes on minimal medium, this was done in rich medium (yeast extract/peptone). Doubling times were calculated by linear regression of log plots of growth curves. R^2 values were >0.95 for all regressions.

Light microscopy

Yeast growing in log phase were examined with a confocal microscopy system (AOBS SP2; Leica) at room temperature (63× NA 1.4 objective) using LCS software (Leica) for acquisition and Photoshop (Adobe) to increase levels uniformly within experiments. For unbiased imaging of cER in mutant strains, transmission imaging was used to focus on the central plane of cells before capturing fluorescence images. To test a strain for polarized

localization of Scs2ΔTMD-GFP, nine random fields of cells (~100 cells per field) were examined, and polarized fluorescence was compared with the wild-type parental strain within each experiment.

Electron microscopy

Cells growing in log phase were studied ultrastructurally using permanganate fixation and uranyl acetate to highlight membranes, including cER, as previously described (Prinz et al., 2000; Fehrenbacher et al., 2002). Thin sections were counterstained and viewed on a transmission electron microscope (model 1010; JEOL).

Morphometry

To determine the axial ratio for a particular strain, multiple differential interference contrast images were taken of the strain, using the same microscope magnification throughout. For every whole cell profile included, the long axis was chosen and marked, and the short axis was then drawn at right angles at the broadest part of the cell. Mothers and unbudded cells were grouped together, and buds were analyzed separately. Mean axial ratio was typically calculated for 200–300 cells.

Quantitation of cER

To quantify cER in fluorescent images, we determined the proportion of plasma membrane occupied by an ER reporter. On a cell by cell basis, this was estimated by drawing (by hand) both the strands of cER (on fluorescent images) and the whole cell perimeter (on transmission images) and measuring the length of these lines using ImageJ software (National Institutes of Health). For automated quantitation of fluorescent images, cells coexpressing RFP-ER and Psr1(N-term)-GFP markers were imaged using settings that completely separated the two fluorophores, with constant microscope magnification and gain settings to facilitate direct comparison. 8-bit images of random fields of cells were processed by ImageJ as described in Fig. S2.

To quantify cER in electron microscopy images, random fields of cells were photographed and analyzed (using ImageJ) to estimate perimeter and to measure every identifiable section of cER, which was taken to be the electron-dense linear structures near and parallel to the plasma membrane. For each cell, the length of each segment of cER was recorded, and the total amount of cER was expressed as a percentage of the perimeter.

Swe1-myc protein levels

Strains transformed with plasmid DLB2258 to add 12xmyc tags to the C terminus of the genomic copy of Swe1 were grown to mid-log growth phase. Where indicated, cells were supplemented with 200 mM HU for a further 4 h. 1–2 × 10^8 cells were pelleted by centrifugation, lysed directly into 2× sample buffer for SDS-PAGE, and heated at 95°C for 5 min before vortexing with 400–600 μm of glass beads (acid washed). Samples were separated on 10% polyacrylamide gels for Western blot analysis both to determine overall Swe1-myc levels with anti-myc (monoclonal 9E10) and to control for loading by probing with antiphosphoglycerate kinase antibody (monoclonal; Invitrogen). In addition, samples were separated on 7% SDS-PAGE without SDS in the separating gel to examine slowly migrating phosphorylated forms of Swe1 (Sakchaisri et al., 2004). The Gel function of ImageJ was used to quantify the main full-length Swe1-myc bands relative to Pgk1.

SGA analysis

SGA analysis was performed as described previously (Tong and Boone, 2006). In brief, *Δscs2-NatR* and *Δice2- NatR* query strains were generated by PCR-mediated homologous recombination and mated to each strain of the deletion array of nonessential genes using a Singer RoToR high density array robot. After selecting for heterozygous diploids, cells were sporulated, and *MATa* haploid cells were allowed to germinate. Subsequent rounds of selection allowed the growth of double-deletion strains or single-deletion strains as controls. Digital images of plates were obtained, and colony sizes were measured and normalized as previously described (Tong and Boone, 2006). Potential interactions were scored by comparing the area of double mutant colonies with single mutants, and a t statistic was derived for each interaction in which more negative numbers indicate an aggravating interaction and more positive numbers indicate an alleviating interaction. In the analysis of septin-related kinases (Fig. 9 C), the two nonessential septins Shs1 and Cdc10 could not be assayed because of germination defects inherent to these deletion strains. All experiments were performed in triplicate.

Online supplemental material

Fig. S1 shows the effect of *Δscs2* on cER in fields of cells expressing three different markers. Fig. S2 uses a semiautomated method to assess the same effect. Fig. S3 shows the lack of effect of many mutations other than *Δscs2* that are implicated in cER inheritance on overall cER levels. Fig. S4 shows that K40A is active in vivo and that Scs2 forms cER and rounds up cells only when it is embedded in the extranuclear ER. Table S1 shows the effect of mutating candidate genes on the localization of Scs2ΔTM-GFP. Table S2 correlates FFAT binding with bud tip localization in Scs2 mutants. Videos 1 and 2 show the slow movement of cER into the proximal portion of *Δscs2Δbni1* cells. Online supplemental material is available at http://www.jcb.org/cgi/content/full/jcb.200708205/DC1.

We thank Anjana Roy for electron microscopy, with technical assistance from Robin Howes and Peter Munro (all at the University College London Institute of Ophthalmology). We also thank Rob Arkowitz, Erfei Bi, Ken Blumer, Charlie Boone, Guenther Daum, Danny Lew, Karl Matter, Yoshikazu Ohya, Hugh Pelham, and Jeremy Thorner for reagents.

This work was supported by the Biotechnology and Biological Sciences Research Council (grant 31/C15982), the Canadian Institutes of Health Research, the Canada Foundation for Innovation, the British Columbia Knowledge Development Fund, the Michael Smith Foundation for Health Research (grant to C.J.R. Loewen), and Fight For Sight.

Submitted: 30 August 2007
Accepted: 5 October 2007

References

Arkowitz, R.A., and N. Lowe. 1997. A small conserved domain in the yeast Spa2p is necessary and sufficient for its polarized localization. *J. Cell Biol.* 138:17–36.

Ayscough, K.R., J. Stryker, N. Pokala, M. Sanders, P. Crews, and D.G. Drubin. 1997. High rates of actin filament turnover in budding yeast and roles for actin in establishment and maintenance of cell polarity revealed using the actin inhibitor latrunculin-A. *J. Cell Biol.* 137:399–416.

Bardo, S., M.G. Cavazzini, and N. Emptage. 2006. The role of the endoplasmic reticulum Ca2+ store in the plasticity of central neurons. *Trends Pharmacol. Sci.* 27:78–84.

Barral, Y., M. Parra, S. Bidlingmaier, and M. Snyder. 1999. Nim1-related kinases coordinate cell cycle progression with the organization of the peripheral cytoskeleton in yeast. *Genes Dev.* 13:176–187.

Beilharz, T., B. Egan, P.A. Silver, K. Hofmann, and T. Lithgow. 2003. Bipartite signals mediate subcellular targeting of tail-anchored membrane proteins in *Saccharomyces cerevisiae*. *J. Biol. Chem.* 278:8219–8223.

Berridge, M.J. 2002. The endoplasmic reticulum: a multifunctional signaling organelle. *Cell Calcium*. 32:235–249.

Berridge, M. 2004. Conformational coupling: a physiological calcium entry mechanism. *Sci. STKE*. doi:10.1126/stke.2432004pe33.

Bonilla, M., and K.W. Cunningham. 2003. Mitogen-activated protein kinase stimulation of Ca(2+) signaling is required for survival of endoplasmic reticulum stress in yeast. *Mol. Biol. Cell*. 14:4296–4305.

Brickner, J.H., and P. Walter. 2004. Gene recruitment of the activated INO1 locus to the nuclear membrane. *PLoS Biol.* 2:e342.

Buvelot Frei, S., P.B. Rahl, M. Nussbaum, B.J. Briggs, M. Calero, S. Janeczko, A.D. Regan, C.Z. Chen, Y. Barral, G.R. Whittaker, and R.N. Collins. 2006. Bioinformatic and comparative localization of rab proteins reveals functional insights into the uncharacterized GTPases Ypt10p and Ypt11p. *Mol. Cell. Biol.* 26:7299–7317.

Clotet, J., X. Escote, M.A. Adrover, G. Yaakov, E. Gari, M. Aldea, E. de Nadal, and F. Posas. 2006. Phosphorylation of Hsl1 by Hog1 leads to a G2 arrest essential for cell survival at high osmolarity. *EMBO J.* 25:2338–2346.

Collin, T., A. Marty, and I. Llano. 2005. Presynaptic calcium stores and synaptic transmission. *Curr. Opin. Neurobiol.* 15:275–281.

Craven, R.J., and T.D. Petes. 2001. The *Saccharomyces cerevisiae* suppressor of choline sensitivity (SCS2) gene is a multicopy Suppressor of mec1 telomeric silencing defects. *Genetics*. 158:145–154.

Cuperus, G., and D. Shore. 2002. Restoration of silencing in *Saccharomyces cerevisiae* by tethering of a novel Sir2-interacting protein, Esc8. *Genetics*. 162:633–645.

De Craene, J.O., J. Coleman, P. Estrada de Martin, M. Pypaert, S. Anderson, J.R. Yates III, S. Ferro-Novick, and P. Novick. 2006. Rtn1p is involved in structuring the cortical ER. *Mol. Biol. Cell*. 17:3009–3020.

Du, Y., M. Pypaert, P. Novick, and S. Ferro-Novick. 2001. Aux1p/Swa2p is required for cortical endoplasmic reticulum inheritance in *Saccharomyces cerevisiae*. *Mol. Biol. Cell*. 12:2614–2628.

Du, Y., S. Ferro-Novick, and P. Novick. 2004. Dynamics and inheritance of the endoplasmic reticulum. *J. Cell Sci.* 117:2871–2878.

Du, Y., L. Walker, P. Novick, and S. Ferro-Novick. 2006. Ptc1p regulates cortical ER inheritance via Slt2p. *EMBO J*. 25:4413–4422.

Endo, S., S. Kubota, H. Siomi, A. Adachi, S. Oroszlan, M. Maki, and M. Hatanaka. 1989. A region of basic amino-acid cluster in HIV-1 Tat protein is essential for trans-acting activity and nucleolar localization. *Virus Genes*. 3:99–110.

Estrada, P., J. Kim, J. Coleman, L. Walker, B. Dunn, P. Takizawa, P. Novick, and S. Ferro-Novick. 2003. Myo4p and She3p are required for cortical ER inheritance in *Saccharomyces cerevisiae*. *J. Cell Biol.* 163:1255–1266.

Estrada de Martin, P., Y. Du, P. Novick, and S. Ferro-Novick. 2005. Ice2p is important for the distribution and structure of the cortical ER network in *Saccharomyces cerevisiae. J. Cell Sci.* 118:65–77.

Evangelista, M., D. Pruyne, D.C. Amberg, C. Boone, and A. Bretscher. 2002. Formins direct Arp2/3-independent actin filament assembly to polarize cell growth in yeast. *Nat. Cell Biol.* 4:260–269.

Evangelista, M., S. Zigmond, and C. Boone. 2003. Formins: signaling effectors for assembly and polarization of actin filaments. *J. Cell Sci.* 116:2603–2611.

Fehrenbacher, K.L., D. Davis, M. Wu, I. Boldogh, and L.A. Pon. 2002. Endoplasmic reticulum dynamics, inheritance, and cytoskeletal interactions in budding yeast. *Mol. Biol. Cell*. 13:854–865.

Gavin, A.C., M. Bosche, R. Krause, P. Grandi, M. Marzioch, A. Bauer, J. Schultz, J.M. Rick, A.M. Michon, C.M. Cruciat, et al. 2002. Functional organization of the yeast proteome by systematic analysis of protein complexes. *Nature*. 415:141–147.

Gladfelter, A.S., L. Kozubowski, T.R. Zyla, and D.J. Lew. 2005. Interplay between septin organization, cell cycle and cell shape in yeast. *J. Cell Sci.* 118:1617–1628.

Harrison, J.C., E.S. Bardes, Y. Ohya, and D.J. Lew. 2001. A role for the Pkc1p/Mpk1p kinase cascade in the morphogenesis checkpoint. *Nat. Cell Biol.* 3:417–420.

Harvey, S.L., and D.R. Kellogg. 2003. Conservation of mechanisms controlling entry into mitosis: budding yeast wee1 delays entry into mitosis and is required for cell size control. *Curr. Biol.* 13:264–275.

Harvey, S.L., A. Charlet, W. Haas, S.P. Gygi, and D.R. Kellogg. 2005. Cdk1-dependent regulation of the mitotic inhibitor Wee1. *Cell*. 122:407–420.

Juschke, C., D. Ferring, R.P. Jansen, and M. Seedorf. 2004. A novel transport pathway for a yeast plasma membrane protein encoded by a localized mRNA. *Curr. Biol.* 14:406–411.

Kadota, J., T. Yamamoto, S. Yoshiuchi, E. Bi, and K. Tanaka. 2004. Septin ring assembly requires concerted action of polarisome components, a PAK kinase Cla4p, and the actin cytoskeleton in *Saccharomyces cerevisiae*. *Mol. Biol. Cell*. 15:5329–5345.

Kaiser, S.E., J.H. Brickner, A.R. Reilein, T.D. Fenn, P. Walter, and A.T. Brunger. 2005. Structural basis of FFAT motif-mediated ER targeting. *Structure*. 13:1035–1045.

Keaton, M.A., and D.J. Lew. 2006. Eavesdropping on the cytoskeleton: progress and controversy in the yeast morphogenesis checkpoint. *Curr. Opin. Microbiol.* 9:540–546.

Lapierre, L.A., P.L. Tuma, J. Navarre, J.R. Goldenring, and J.M. Anderson. 1999. VAP-33 localizes to both an intracellular vesicle population and with occludin at the tight junction. *J. Cell Sci.* 112:3723–3732.

Levine, T.P., and S. Munro. 2001. Dual targeting of Osh1p, a yeast homologue of oxysterol-binding protein, to both the Golgi and the nucleus-vacuole junction. *Mol. Biol. Cell*. 12:1633–1644.

Levine, T.P., and S. Munro. 2002. Targeting of Golgi-specific pleckstrin homology domains involves both PtdIns 4-kinase-dependent and -independent components. *Curr. Biol.* 12:695–704.

Lew, D.J. 2003. The morphogenesis checkpoint: how yeast cells watch their figures. *Curr. Opin. Cell Biol.* 15:648–653.

Loewen, C.J.R., and T.P. Levine. 2005. A highly conserved binding site in VAP for the FFAT motif of lipid binding proteins. *J. Biol. Chem.* 280:14097–14104.

Loewen, C.J., A. Roy, and T.P. Levine. 2003. A conserved ER targeting motif in three families of lipid binding proteins and in Opi1p binds VAP. *EMBO J.* 22:2025–2035.

Loewen, C.J., M.L. Gaspar, S.A. Jesch, C. Delon, N.T. Ktistakis, S.A. Henry, and T.P. Levine. 2004. Phospholipid metabolism regulated by a transcription factor sensing phosphatidic acid. *Science*. 304:1644–1647.

Longtine, M.S., and E. Bi. 2003. Regulation of septin organization and function in yeast. *Trends Cell Biol.* 13:403–409.

Longtine, M.S., C.L. Theesfeld, J.N. McMillan, E. Weaver, J.R. Pringle, and D.J. Lew. 2000. Septin-dependent assembly of a cell cycle-regulatory module in *Saccharomyces cerevisiae*. *Mol. Cell. Biol.* 20:4049–4061.

Luedeke, C., S.B. Frei, I. Sbalzarini, H. Schwarz, A. Spang, and Y. Barral. 2005. Septin-dependent compartmentalization of the endoplasmic reticulum during yeast polarized growth. *J. Cell Biol.* 169:897–908.

Matheos, D., M. Metodiev, E. Muller, D. Stone, and M.D. Rose. 2004. Pheromone-induced polarization is dependent on the Fus3p MAPK acting through the formin Bni1p. *J. Cell Biol*. 165:99–109.

McMillan, J.N., R.A. Sia, and D.J. Lew. 1998. A morphogenesis checkpoint monitors the actin cytoskeleton in yeast. *J. Cell Biol.* 142:1487–1499.

McMillan, J.N., M.S. Longtine, R.A. Sia, C.L. Theesfeld, E.S. Bardes, J.R. Pringle, and D.J. Lew. 1999. The morphogenesis checkpoint in *Saccharomyces cerevisiae*: cell cycle control of Swe1p degradation by Hsl1p and Hsl7p. *Mol. Cell. Biol.* 19:6929–6939.

McMillan, J.N., C.L. Theesfeld, J.C. Harrison, E.S. Bardes, and D.J. Lew. 2002. Determinants of Swe1p degradation in *Saccharomyces cerevisiae*. *Mol. Biol. Cell*. 13:3560–3575.

Mironov, S.L., and N. Symonchuk. 2006. ER vesicles and mitochondria move and communicate at synapses. *J. Cell Sci.* 119:4926–4934.

Nishimura, A.L., M. Mitne-Neto, H.C. Silva, A. Richieri-Costa, S. Middleton, D. Cascio, F. Kok, J.R. Oliveira, T. Gillingwater, J. Webb, et al. 2004. A mutation in the vesicle-trafficking protein VAPB causes late-onset spinal muscular atrophy and amyotrophic lateral sclerosis. *Am. J. Hum. Genet.* 75:822–831.

Pichler, H., B. Gaigg, C. Hrastnik, G. Achleitner, S.D. Kohlwein, G. Zellnig, A. Perktold, and G. Daum. 2001. A subfraction of the yeast endoplasmic reticulum associates with the plasma membrane and has a high capacity to synthesize lipids. *Eur. J. Biochem.* 268:2351–2361.

Poteryaev, D., J.M. Squirrell, J.M. Campbell, J.G. White, and A. Spang. 2005. Involvement of the actin cytoskeleton and homotypic membrane fusion in ER dynamics in *C. elegans*. *Mol. Biol. Cell*. 16:2139–2153.

Prinz, W.A., L. Grzyb, M. Veenhuis, J.A. Kahana, P.A. Silver, and T.A. Rapoport. 2000. Mutants affecting the structure of the cortical endoplasmic reticulum in *Saccharomyces cerevisiae*. *J. Cell Biol.* 150:461–474.

Pruyne, D., and A. Bretscher. 2000. Polarization of cell growth in yeast. I. Establishment and maintenance of polarity states. *J. Cell Sci.* 113:365–375.

Reinke, C.A., P. Kozik, and B.S. Glick. 2004. Golgi inheritance in small buds of *Saccharomyces cerevisiae* is linked to endoplasmic reticulum inheritance. *Proc. Natl. Acad. Sci. USA*. 101:18018–18023.

Rolls, M.M., D.H. Hall, M. Victor, E.H. Stelzer, and T.A. Rapoport. 2002. Targeting of rough endoplasmic reticulum membrane proteins and ribosomes in invertebrate neurons. *Mol. Biol. Cell*. 13:1778–1791.

Roumanie, O., H. Wu, J.N. Molk, G. Rossi, K. Bloom, and P. Brennwald. 2005. Rho GTPase regulation of exocytosis in yeast is independent of GTP hydrolysis and polarization of the exocyst complex. *J. Cell Biol.* 170:583–594.

Saito, T.L., M. Ohtani, H. Sawai, F. Sano, A. Saka, D. Watanabe, M. Yukawa, Y. Ohya, and S. Morishita. 2004. SCMD: *Saccharomyces cerevisiae* Morphological Database. *Nucleic Acids Res.* 32:D319–D322.

Sakchaisri, K., S. Asano, L.R. Yu, M.J. Shulewitz, C.J. Park, J.E. Park, Y.W. Cho, T.D. Veenstra, J. Thorner, and K.S. Lee. 2004. Coupling morphogenesis to mitotic entry. *Proc. Natl. Acad. Sci. USA*. 101:4124–4129.

Sato, M., K. Sato, and A. Nakano. 1996. Endoplasmic reticulum localization of Sec12p is achieved by two mechanisms: Rer1p-dependent retrieval that requires the transmembrane domain and Rer1p-independent retention that involves the cytoplasmic domain. *J. Cell Biol.* 134:279–293.

Schmidt, M., A. Varma, T. Drgon, B. Bowers, and E. Cabib. 2003. Septins, under Cla4p regulation, and the chitin ring are required for neck integrity in budding yeast. *Mol. Biol. Cell*. 14:2128–2141.

Schuldiner, M., S.R. Collins, N.J. Thompson, V. Denic, A. Bhamidipati, T. Punna, J. Ihmels, B. Andrews, C. Boone, J.F. Greenblatt, et al. 2005. Exploration of the function and organization of the yeast early secretory pathway through an epistatic miniarray profile. *Cell*. 123:507–519.

Sekiya-Kawasaki, M., M. Abe, A. Saka, D. Watanabe, K. Kono, M. Minemura-Asakawa, S. Ishihara, T. Watanabe, and Y. Ohya. 2002. Dissection of upstream regulatory components of the Rho1p effector, 1,3-beta-glucan synthase, in *Saccharomyces cerevisiae*. *Genetics*. 162:663–676.

Sheu, Y.J., B. Santos, N. Fortin, C. Costigan, and M. Snyder. 1998. Spa2p interacts with cell polarity proteins and signaling components involved in yeast cell morphogenesis. *Mol. Cell. Biol.* 18:4053–4069.

Shulewitz, M.J., C.J. Inouye, and J. Thorner. 1999. Hsl7 localizes to a septin ring and serves as an adapter in a regulatory pathway that relieves tyrosine phosphorylation of Cdc28 protein kinase in *Saccharomyces cerevisiae*. *Mol. Cell. Biol.* 19:7123–7137.

Siniossoglou, S., E.C. Hurt, and H.R. Pelham. 2000. Psr1p/Psr2p, two plasma membrane phosphatases with an essential DXDX(T/V) motif required for sodium stress response in yeast. *J. Biol. Chem.* 275:19352–19360.

Skehel, P.A., K.C. Martin, E.R. Kandel, and D. Bartsch. 1995. A VAMP-binding protein from Aplysia required for neurotransmitter release. *Science*. 269:1580–1583.

Spiliotis, E.T., and W.J. Nelson. 2006. Here come the septins: novel polymers that coordinate intracellular functions and organization. *J. Cell Sci.* 119:4–10.

Sutterlin, C., P. Hsu, A. Mallabiabarrena, and V. Malhotra. 2002. Fragmentation and dispersal of the pericentriolar Golgi complex is required for entry into mitosis in mammalian cells. *Cell*. 109:359–369.

Suzuki, M., R. Igarashi, M. Sekiya, T. Utsugi, S. Morishita, M. Yukawa, and Y. Ohya. 2004. Dynactin is involved in a checkpoint to monitor cell wall synthesis in *Saccharomyces cerevisiae*. *Nat. Cell Biol.* 6:861–871.

Tong, A.H., and C. Boone. 2006. Synthetic genetic array analysis in *Saccharomyces cerevisiae*. *Methods Mol. Biol.* 313:171–192.

Verges, E., N. Colomina, E. Gari, C. Gallego, and M. Aldea. 2007. Cyclin Cln3 is retained at the ER and released by the J chaperone Ydj1 in late G1 to trigger cell cycle entry. *Mol. Cell*. 26:649–662.

Versele, M., and J. Thorner. 2004. Septin collar formation in budding yeast requires GTP binding and direct phosphorylation by the PAK, Cla4. *J. Cell Biol.* 164:701–715.

Voeltz, G.K., M.M. Rolls, and T.A. Rapoport. 2002. Structural organization of the endoplasmic reticulum. *EMBO Rep.* 3:944–950.

Voeltz, G.K., W.A. Prinz, Y. Shibata, J.M. Rist, and T.A. Rapoport. 2006. A class of membrane proteins shaping the tubular endoplasmic reticulum. *Cell*. 124:573–586.

Wiederkehr, A., Y. Du, M. Pypaert, S. Ferro-Novick, and P. Novick. 2003. Sec3p is needed for the spatial regulation of secretion and for the inheritance of the cortical endoplasmic reticulum. *Mol. Biol. Cell*. 14:4770–4782.

Zweytick, D., E. Leitner, S.D. Kohlwein, C. Yu, J. Rothblatt, and G. Daum. 2000. Contribution of Are1p and Are2p to steryl ester synthesis in the yeast *Saccharomyces cerevisiae*. *Eur. J. Biochem.* 267:1075–1082.